

Electron- D^0 Correlations With ALICE

In pp Collisions At LHC Energy

Dem Fachbereich Physik der
Technischen Universität Darmstadt

zur Erlangung des Grades eines
Doktors der Naturwissenschaften
(Dr. rer. nat.)

genehmigte Dissertation von

Dipl.-Phys Sedat Altınpınar

aus Wülfrath

GSI Helmholtzzentrum für Schwerionenforschung

Referent: Prof. Dr. Peter Braun-Munzinger

Korreferent: Prof. Dr. Jochen Wambach

Tag der Einreichung: 12.7.2011

Tag der Prüfung: 14.11.2011

Darmstadt 2011

D17

Abstract

With ALICE at LHC a new energy domain of Quark-Gluon Plasma physics can be explored. Partonic energy loss studies are one of the major investigation methods, which can reveal important information about the interaction of quarks and gluons in the mentioned state of matter. To employ heavy quarks as probes is especially suited for this purpose, since they are created early in nucleus-nucleus collisions and experience the full collision history. An additional distinction between charm or bottom quarks contributes to refine the understanding of partonic energy loss. For this aim a separation method called factorization is developed. This analysis is based on the angular correlation of electrons from heavy-flavor hadron decays and D^0 mesons, depending on the topology of underlying QCD processes. The purpose is to obtain a momentum dependent charm to beauty cross section ratio in proton-proton collisions, which is a baseline for the lead-lead collisions and an essential input for partonic energy loss models. The analysis presented is a groundwork, showing how such an analysis can be done in ALICE. Precondition of such kind of analysis are the reconstruction of D^0 mesons and the identification and selection of electrons from heavy-flavor hadron decays. First D^0 mesons in ALICE are measured, by developing a particle identification strategy for the $D^0 \rightarrow K\pi$ decay mode and kinematical selection criteria for the mentioned two daughter particles. Moreover the measured D^0 mesons provide the possibility to make comparisons with perturbative QCD cross section calculations and check their agreement. Conclusions on the statistical model are possible as well, with the measurement of the ratio of neutral and charged D mesons. Also a preliminary selection strategy to separate electrons from heavy-flavor hadron decays from other electrons is worked out and a novel background subtraction technique of non-heavy flavor background in the correlation distribution is presented as well. Since this analysis is very statistics-hungry, there is currently no statistically conclusive correlation plot possible, with the present amount of collected events. Nevertheless, a first evaluation employing the factorization method is done.

Zusammenfassung

Mit ALICE am LHC kann ein neuer Energiebereich des Quark-Gluon Plasmas erforscht werden. Studien über partonischen Energieverlust sind einige der grundlegenden Untersuchungsmethoden, welche wichtige Informationen über die Wechselwirkung von Quarks und Gluonen in dem genannten Materiezustand enthüllen können. Der Einsatz von schweren Quarks als Sonden ist für diese Zwecke besonders geeignet, da sie in Kern-Kern Stößen früh erzeugt werden und somit die volle Kollisionentwicklung durchleben. Eine zusätzliche Unterscheidung zwischen Charm- und Beauty-Quarks trägt zur Vertiefung des Verständnisses über partonischen Energieverlust bei. Für diesen Zweck der Separation wurde eine Faktorisierungsmethode entwickelt. Diese Analyse beruht auf der Winkelkorrelation von Elektronen aus Schwere-Quark-Hadronenzerfällen und D^0 Mesonen, abhängig von dem zugrundeliegenden QCD Prozess. Das Ziel ist es ein impulsabhängiges Charm zu Beauty Wirkungsquerschnitt-Verhältnis in Proton-Proton Stößen zu ermitteln, welches eine Referenz für Blei-Blei Stöße darstellt und als essentielle Größe für partonische Energieverlustmodelle eingeht. Die präsentierte Analyse ist eine Basisarbeit, die zeigt wie solch eine Analyse in ALICE realisiert werden kann. Voraussetzung für so eine Analyse ist die Rekonstruktion von D^0 Mesonen und die Identifizierung und Selektion von Elektronen aus Schwere-Quark-Hadronenzerfällen. Durch die Entwicklung einer Strategie zur Teilchenidentifizierung für den Zerfallskanal $D^0 \rightarrow K\pi$ und kinematischen Auswahlkriterien für die genannten zwei Zerfallsteilchen, wurden erste D^0 Mesonen in ALICE gemessen. Die gemessenen D^0 Mesonen bieten außerdem die Möglichkeit Vergleiche mit pQCD Wirkungsquerschnitt Berechnungen zu ziehen und ihre Übereinstimmungen zu prüfen. Mit der Messung des Verhältnisses neutraler und geladener D Mesonen sind Schlussfolgerungen zum Statistischen Modell möglich. Eine erste Version einer Selektionsstrategie um Elektronen aus Hadronenzerfällen die schwere Quarks enthalten von anderen Elektronen zu trennen wurde ausgearbeitet und eine neuartige Hintergrundsubtraktionsmethode für Elektronen aus Hadronenzerfällen die nur leichte Quarks enthalten und zu den Korrelationsverteilungen beitragen, sind ebenfalls präsentiert. Da diese Analyse sehr große Statistik bedarf, ist mit der aktuellen Menge von Ereignissen eine statistisch schlüssige Korrelationsverteilung nicht möglich. Dennoch wurde eine erste Bewertung mit der Faktorisierungsmethode durchgeführt.

Contents

1	Introduction	9
1.1	The Quark-Gluon Plasma	10
2	The ALICE Setup	17
3	Theory and Motivation of Angular Correlations	27
3.1	Partonic Energy Loss	29
3.2	Quark-Fragment Parity Inheritance	30
3.3	Topology of Leading Order Processes	31
3.4	Correlations in η - φ Space	32
4	Angular Electron-Hadron Correlation Methods	37
4.1	Shape Fitting Method	37
4.2	Angular Separation by Charge Sign Condition Method	38
4.3	A New Method: Factorization	40
5	Angular Correlation Analysis	49
5.1	D^0 Reconstruction	50
5.1.1	Conclusions from the D^0 Reconstruction	54
5.2	Electron Selection	56
5.3	Correlation Analysis	63
6	Conclusion and Outlook	69
A	Parallel coordinates	71
B	Single contribution type for Factorization Method	74

List of Figures

1.1	Image of background cosmic radiation by WMAP(Wilkinson Microwave Anisotropy Probe)	10
1.2	QCD phase diagram	13
1.3	R_{AA} spectra measured by ALICE, STAR and PHENIX experiments in central collisions	14
2.1	Time evolution of colliding nuclei	18
2.2	ALICE Setup	19
2.3	Two views of the ITS with its 3 double layer detectors	20
2.4	Transverse impact parameter resolution as a function of transverse momentum	21
2.5	Schematic working principle of the Time Projection Chamber (TPC)	23
2.6	dE/dx as a function of momentum of particles traversing the TPC and Bethe-Bloch functions for different particle species	24
2.7	Particle separation power for individual detectors as a function of momentum	26
3.1	PHENIX single electron spectrum in 200 GeV center-of-mass pp collisions and FONLL calculations	28
3.2	Parity relation of the c quark and decay electrons	30
3.3	Charm quark changes flavor to strange under the emission of a W^- boson, which decays subsequently into an electron neutrino pair	30
3.4	Main production processes of heavy flavor	31
3.5	Angular distributions of single production processes for $c\bar{c}$ pairs in $\sqrt{s}= 7$ TeV pp collisions obtained from PYTHIA	32
3.6	Narrow real angle (opening angle) in full space between the produced charm and anti-charm quarks, due to the relativistic boost in their production at LHC energies and longitudinal momentum relation of $c\bar{c}$ pairs	33
3.7	Transverse and longitudinal momentum relation for c quarks	33

3.8	Incoming protons at relativistic energies and relation transverse vs longitudinal momentum of outgoing collision products	34
3.9	Angular Correlation for $c\bar{c}$ pairs in $\Delta\varphi$ and d variable	34
3.10	Angular Correlations for $b\bar{b}$ pairs in $\Delta\varphi$ and d variable	35
4.1	Correlations measured at STAR	38
4.2	Azimuthal distribution of $c\bar{c}$ pairs and $b\bar{b}$ pairs	39
4.3	Illustration of decay topology of example charm and beauty quark fragmentation	40
4.4	Angular distribution simulations and evaluation formulas in angular separation by charge sign condition method	41
4.5	Example decay stems for a $c\bar{c}$ and $b\bar{b}$ pair	42
4.6	Hadron fractions containing charm or beauty quarks	43
4.7	List of e- D^0 contributions	44
4.8	List of e- \bar{D}^0 contributions	45
5.1	D^0 Invariant mass distributions in 3 p_t bins	54
5.2	D^0 raw yields in 3 p_t bins	55
5.3	D^0 production cross section as function of p_t and comparison with FONLL and GM-VFNS calculations	56
5.4	Measurements of experiments and MNR (pQCD) calculation for the total charm cross section per nucleon-nucleon collision as a function of center-of-mass system energy	57
5.5	D^0/D^+ ratio as a function of p_t	58
5.6	Charged to neutral D meson cross section ratios as function of center-of-mass energy in elementary hadron collisions with comparison to statistical model calculation	59
5.7	Hadron contamination of electrons as a function of momentum	60
5.8	Evolution of statistics entries vs. cuts	61
5.9	Inclusive electron spectrum and cocktail	62
5.10	Ratio obtained from inclusive electron spectrum and cocktail as a function of p_t	64
5.11	Electrons correlated with D^0 candidates in the peak region	65
5.12	Electrons correlated with D^0 candidates in the sideband	65
5.13	Electrons correlated with \bar{D}^0 candidates in the peak region	66
5.14	Electrons correlated with \bar{D}^0 candidates in the sideband	66
A.1	Example six dimensional point (-5,3,4,2,0,1) in parallel coordinates	71
A.2	Parallel coordinates used in order to tune globally the selection D^0 cuts	72

B.1 Illustration of the formation of a single contribution type in the
angular correlation function 75

Chapter 1

Introduction

The question “Where do we come from?” is probably as old as the human himself. Research in the area of first moments of the universe, is giving answers to even more basic questions than how life appeared, namely how matter started to exist. The impressive image (Figure 1.1) of the Cosmic Microwave Background, shortly CMB, which is a snapshot from the time, where the universe became transparent roughly 400.000 years after the big bang, shows a direct way to access experimentally early stages of the cosmos. This way of looking back in time is indeed formidable, however there is an even earlier stage, which can be investigated experimentally. On the way from the Quark epoch to the Hadron epoch, there was a phase of matter called Quark-Gluon Plasma (QGP), which is described in more detail in the next section 1.1. This kind of matter can be recreated by smashing nuclei at very high energy. The tool, providing such circumstances are accelerators. Currently the accelerator LHC¹ at CERN² is delivering with 7 TeV center-of-mass energy for proton-proton collisions and 2.76 TeV per nucleon pair in lead-lead collisions, the highest energy available worldwide. This amazing energy produces in the collisions a temperature circa 500.000 times higher than the Sun’s core [NDH⁺11], which is needed to create the mentioned QGP. This primordial soup which was already created at SPS³ and later at RHIC⁴, will be hotter, last longer and will give possibility to investigate the physical properties in depth and will be a window to reveal new knowledge.

It should be noted, that the understanding of the QGP doesn’t contribute only to cosmological aspects; it also adds to explain, how nature works at partonic level or in other words, what are the properties of basic matter.

¹Large Hadron Collider

²Centre Européen pour la Recherche Nucleaire

³Super Proton Synchrotron

⁴Relativistic Heavy Ion Collider

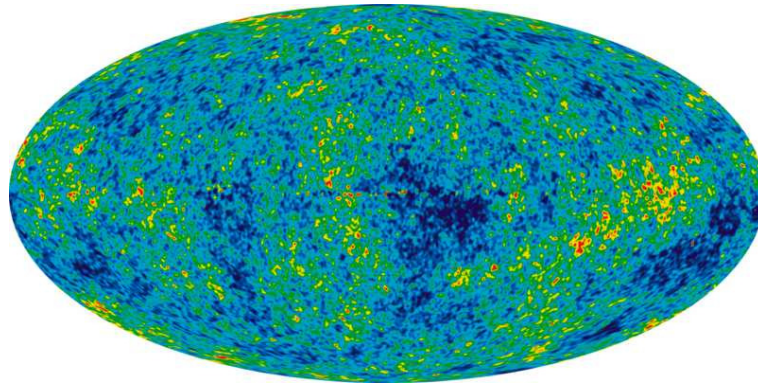


Figure 1.1: Image of background cosmic radiation by WMAP(Wilkinson Microwave Anisotropy Probe). The average temperature is 2.725 Kelvin and the fluctuations are about 0.0002 Kelvin. [Tea]

ALICE⁵, one of the four big experiments at LHC, is a dedicated heavy-ion experiment, that is to say it is designed especially to investigate the QGP. Some important features of ALICE are described in chapter 2.

1.1 The Quark-Gluon Plasma

If one goes deeper and deeper in the structure of matter, one arrives at nucleons, which contain quarks. The attempt to split nucleons, or rather hadrons in general, and get an isolated quark out of it, is the point, where one hits the wall. The energy, which one pumps into the system, in order to separate the $q\bar{q}$ pair, creates after a certain point a new $q\bar{q}$ pair, since it is energetically more favorable, than stretching more the color flux between the initial quarks. The reason for this interesting behavior is the nature of the force interacting between the quarks, which is described by Quantum Chromodynamics (QCD). As the name of the theory tells, the charge responsible for the *strong interaction* are colors, which is an additional degree of freedom of quarks. The interaction can be explained in a naive example like the following: Let's imagine a quark with blue charge which is interacting with another quark with green charge. The blue quark emits a gluon with blue + antigreen charge. The emitting quark is left with green in this case. The receiving quark will convert its charge from green to blue. As result the charges will be swapped. This simple example indicates already some properties of a non-Abelian gauge theory, as it is QCD. Let's explain the non-Abelian gauge theory in a simplified way.

⁵A Large Ion Collider Experiment

Gauge theory it is called because the forces emerge out of the requirement, that the Lagrangian has to stay invariant under a local gauge transformation. In a simplified version the gauge transformation can be explained with the following analogy: Imagine a fluid with the possibility to have some dynamics. Let's look at a place, where is no hydrodynamical flow. Now we set at this place a new reference instead of zero as volumetric flow rate and at another place we set a different reference value (setting local colors). Now to restore the initial situation it is necessary to set also a flow among the two places, which corresponds in our analogy to the emerging force. The name of the theory comes from this idea of *gauging*. As a remark aside, that the gluons don't have mass, comes also from the invariance requirement of the Lagrangian; massive gluons would break the invariance [Won94].

Non-Abelian means, that the field operators don't commute, i.e. that it matters in which order one applies blue, green etc. A visible feature in the example is also that the gluon itself has color. In Quantumelectrodynamics (QED) this would correspond to the situation, that the photon carries electrical charge, what is not suiting the gauge group U(1). The gauge group in which the gluons can be represented properly is SU(3), where one has also the non-Abelian feature of non-commuting operators. Moreover a non-Abelian gauge theory describes an interaction system which is getting strong on large distance scales [Won94]. This effect results in a so-called infrared slavery, which confines the quarks in hadrons, as mentioned before.

Nevertheless there is still a possible (Nobel prize awarded) trick to liberate the quark from its hadron. For this, first we ask the question: What happens in the other extreme, contrary to the infrared slavery, if quarks approach each other? Gross and Wilczek answered this question in their publication with the title: Ultraviolet behavior of non-Abelian gauge theories [GW73] (Politzer shared the Nobel Prize with Gross and Wilczek for the discovery [Pol73]). As shown there, these theories have a free-field-theory asymptotic behavior. In this case the QCD coupling constant follows the relation [Won94], [GW73]:

$$\alpha(q^2) = \frac{\alpha_0}{1 + \alpha_0 \frac{(33-2n_f)}{12\pi} \ln\left(\frac{-q^2}{\mu^2}\right)} \quad (1.1)$$

with the following variables:

α ,	Coupling constant
q ,	Momentum transfer
α_0, μ ,	α_0 Coupling constant for the momentum transfer μ
n_f ,	Number of flavors

As visible in Eq. 1.1, the coupling constant decreases at high momentum transfers, i.e. short distances, which is called asymptotic freedom. According to [Lex00], the Quark-Gluon Plasma (QGP) is a state of hadronic matter at very high energy densities in the order of $1 \text{ GeV}/\text{fm}^3$, where quarks and gluons interact as individual particles, obeying the laws of quantumchromodynamics. This is what occurs in the regime of asymptotic freedom. Quarks lose their host hadron identity and are able to roam over several Debye lengths, in the terminology of plasma physics. In Figure 1.2 the phase diagram of this strongly interacting matter is shown.

The transition to the QGP, i.e. the deconfinement of quarks, happens at high temperature or/and at high baryochemical potential. The values at which the transition occurs are obtained from thermal fits within the statistical model [ABMS10]. These fits are performed by measuring hadron yields and drawing conclusions from the baryochemical potential and the temperature at hadronization or in other words the freeze-out, which are parameters of the mentioned model. The limiting temperature is found to be $T_{lim} = 165 \text{ MeV}$, which implies that matter above this temperature is in the mentioned QGP state. The transition to the deconfined phase will be at LHC at a temperature close to the limiting temperature and as can be read from Figure 1.2 accordingly at very low baryochemical potential, as it happend similarly in the early universe.

Once the deconfined phase is created in nucleus-nucleus collisions, it can be studied with a variety of signatures. One of these signatures is the suppression of particle production at high transverse momentum (p_t). High p_t hadrons are originating from partons, produced predominantly in hard scattering processes. The suppression of the high p_t hadrons can occur due to energy loss, which the corresponding partons experience, while traversing the Quark-Gluon Plasma. The suppression is quantified by the observable R_{AA} , the so-called nuclear modification factor, as defined in Eq. 1.2.

$$R_{AA}(p_t) = \frac{\sigma_{AA}(p_t)}{\langle N_{binary} \rangle \sigma_{NN}(p_t)} \quad (1.2)$$

The variables are:

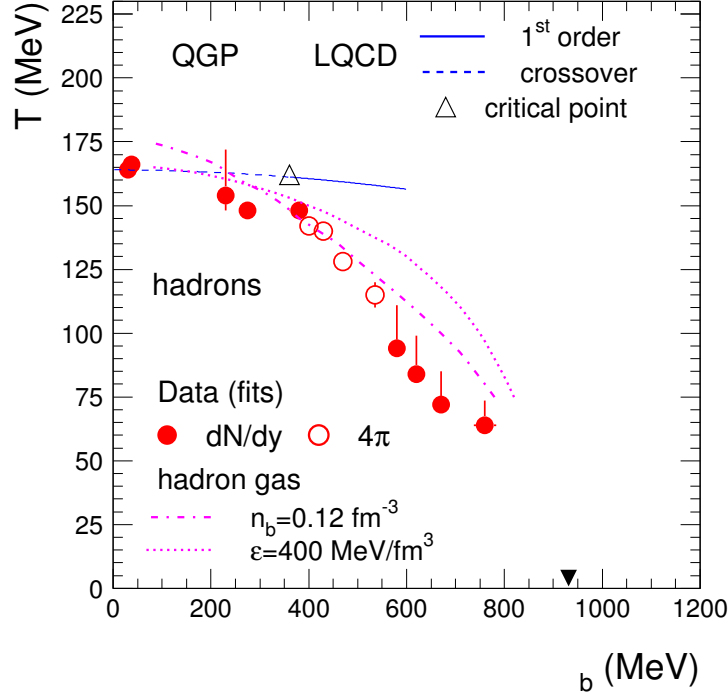


Figure 1.2: Phase diagram of QCD matter in dependence on temperature and baryochemical potential. The data points are thermal fit values, obtained from measured hadron yields, evaluated with the statistical model [ABMS10]. Full circles indicate midrapidity fit results and empty ones fit results for full phase space. Calculations from lattice QCD⁶[FK04] and freeze-out curves of a hadron gas at fix baryon and energy density are displayed as well. The triangle at zero temperature indicates the state of nuclear matter in atomic nuclei. [ABMS10]

$$\sigma_{AA/NN}(p_t), \quad p_t \text{ distribution from AA or pp collisions}$$

$$\langle N_{binary} \rangle, \quad \text{Number of primary nucleon-nucleon collisions}$$

$\langle N_{binary} \rangle$ is obtained from the inelastic NN (nucleon-nucleon) cross section and the nuclear overlap function based on the Glauber model [YHM05]. The idea of R_{AA} is to measure the impact of the medium in AA (nucleus-nucleus) collisions

⁶Lattice QCD is a formulation of QCD on the lattice, allowing for a numerical solution.

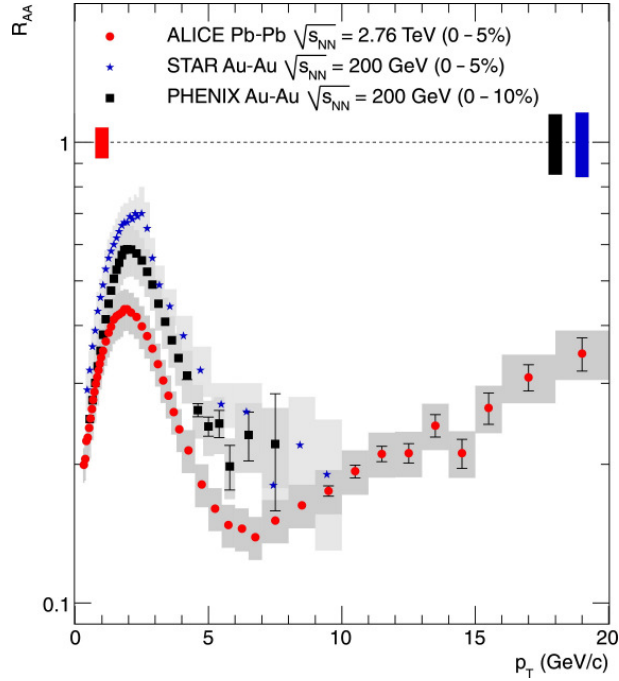


Figure 1.3: R_{AA} spectra measured by ALICE, STAR and PHENIX experiments in central collisions. Error bars represent statistical and boxes the systematic uncertainties, except for STAR where both error types are combined and shown as boxes. p_t independent R_{AA} scaling errors are displayed as bars on the dashed line. [Col11]

on particle yields. For this the yield in NN collisions (here proton-proton (pp) collisions) is scaled with the number of binary nucleon collisions in corresponding AA collisions in a given centrality class. This scaled yield is compared with the yield in the according AA collisions. If there is no medium effect, the ratio of the two yields is unity. The case of a value lower than one indicates a suppression. It should be noted that the scaling with $\langle N_{binary} \rangle$ in the sector of soft production processes is not valid but rather the scaling has to be done with the number of participant nucleons $\langle N_{part} \rangle$. This is also the reason that in R_{AA} distributions which are scaled over the whole p_t range with $\langle N_{binary} \rangle$, the low p_t region doesn't exceed one, while in the high p_t region the values are also below one. The R_{AA} spectrum measured at STAR and PHENIX, which are two experiments at RHIC, together with the current ALICE measurements are shown in Figure 1.3. High p_t suppression was first observed at RHIC, operated with gold ions colliding at 200 GeV center-of-mass energy per nucleon pair, whereas ALICE probes a new energy domain currently at 2.76 TeV, using lead ions (design center-of-mass energy is 5.5 TeV). Since there is currently no data from pp collisions at 2.76 TeV, the reference

distribution is obtained by interpolating ALICE pp data, taken at 0.9 and 7 TeV center-of-mass energy.

It is visible that high p_t suppression is seen at the LHC higher than at RHIC at around 6 GeV/c, which indicates an increased partonic energy loss and consequently a denser medium (partonic energy loss is explained in more detail in section 3.1). Moreover it was expected according to the recombination model [FM04], that the peak in the R_{AA} distribution at $p_t \sim 2$ GeV/c will be shifted at LHC energies to higher transverse momenta. This prediction, based on the concept of an extension of soft thermal physics to higher p_t 's is disproved, since the shape and position of the mentioned ALICE peak agrees with the ones from RHIC. What also stands out in Figure 1.3, is that by ALICE the p_t reach of the R_{AA} spectrum is more than doubled up to 20 GeV/c. In the p_t region above 7 GeV/c, there is a clear increasing trend visible. A quantitative conclusion on partonic energy loss needs further theoretical investigations and modeling.

Another facet and contribution to the understanding of partonic energy loss is presented in the next chapters.

Chapter 2

The ALICE Setup

ALICE is the experiment specially designed to study the Quark-Gluon Plasma, mentioned in the previous chapter. Particle physics experiments are designed, among other criteria, according to key properties like: energy regime, momentum and direction of detectable particles and their identification. In this respect ALICE is tuned to the expected signatures of the QGP at LHC conditions, in contrast to the other three big experiments at LHC, which are tuned for proton-proton collisions. A major feature of ALICE is in this regard its capabilities in a high multiplicity environment.

In the collisions of nuclei with sufficient energy, the QGP is created but lives very shortly. The QGP hadronizes and thus provides the particles, which one can see in the various detectors. Consequently, informations about the QGP can be obtained in this way only indirectly. The phases of the collisions are depicted in Figure 2.1. The task of ALICE is to measure the mentioned hadrons via their decay products plus leptons and photons, coming directly from the fireball and understand signatures, which are typical for the QGP. These can be for example momentum distributions of certain hadrons or leptons, production enhancement or suppression of particles or correlations of those. The tracking and identification of these particles is done in ALICE, starting from low momentum around $100 \text{ MeV}/c$ up to very high momentum at $\sim 100 \text{ GeV}/c$, meaning an impressive dynamic momentum range of three orders of magnitude [Col04]. Also the spatial resolution of the primary vertex below 100 microns (in the plane perpendicular to the beam axis) is essential in order to reconstruct D and B mesons, which plays a major role in the analysis, presented in this thesis. On top on that, all this has to be performed in a high multiplicity environment. At LHC charged particle multiplicities up to a maximum of 8000 per pseudorapidity unit are expected [Col04] at the design center of mass energy of 5.5 TeV per nucleon pair in lead-lead collisions. Theoretical predictions range between 2000 and 6000 for the mentioned energy, where a design value of 8000 ensures a reliable safety margin [Col04].

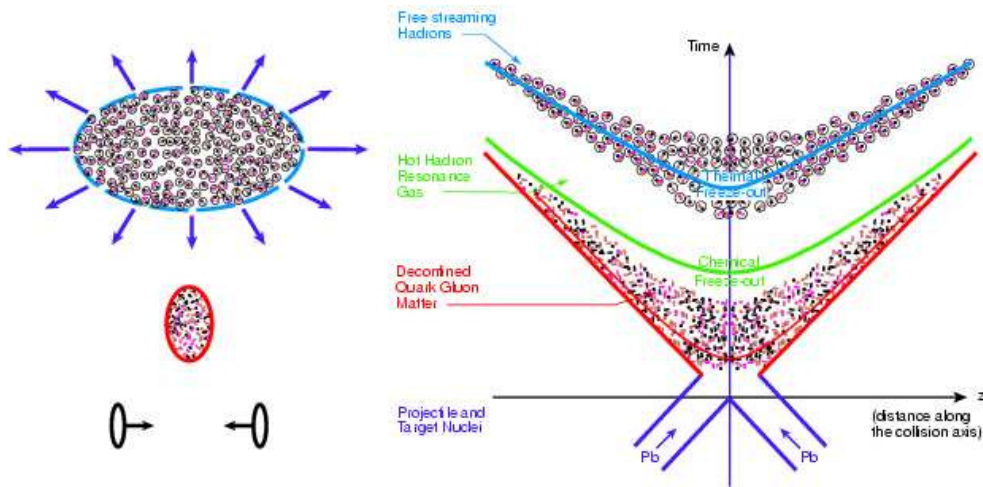


Figure 2.1: Time evolution of colliding nuclei [NA4]. The QGP is created already after 1 fm/c. After about a few fm/c the hadronization starts, referred to as chemical freeze-out and after additional few fm/c, thermal freeze-out occurs. After this stage there is no strong interaction acting among the hadrons anymore, which travel then to the detectors.

A measurement of ALICE at 2.76 TeV delivered a charged particle multiplicity density at mid-rapidity of 1584 ± 4 (stat.) ± 76 (sys.) [Aam10]. By a projection with a power law based on the center of mass energy $\propto s_{NN}^{0.15}$, including data from other experiments, the charged particle multiplicity density is roughly 2000 for lead-lead collisions at 5.5 TeV. ALICE is designed for a luminosity value of $10^{27} \text{ cm}^{-2} \text{ s}^{-1}$ for lead-lead collisions, what results in a detector configuration which is designed with more priority for high-granularity than for speed.

As visible in Figure 2.2, ALICE consists of two major parts: The central barrel and the muon arm.

Roughly described, the central barrel consists of cylindrical concentric detectors starting with a vertexing detector, around the beam pipe -the ITS, which enables precise tracking, surrounded by a minimal multiple scattering environment, namely a detector with huge gaseous volume -the TPC which is again surrounded by more specific detectors, supporting the tracking and having specific particle identification tasks -e.g. TRD and TOF.

The full azimuthal coverage plays an essential role for an analysis of angular correlations, as it is the case of this thesis. Moreover to reconstruct particles with low momentum (big opening angle) decay products, it is also important to have full azimuthal coverage. Another coverage which is relevant, is the extension along the beam pipe, which is covered by the central barrel, for a pseudorapidity

ALICE

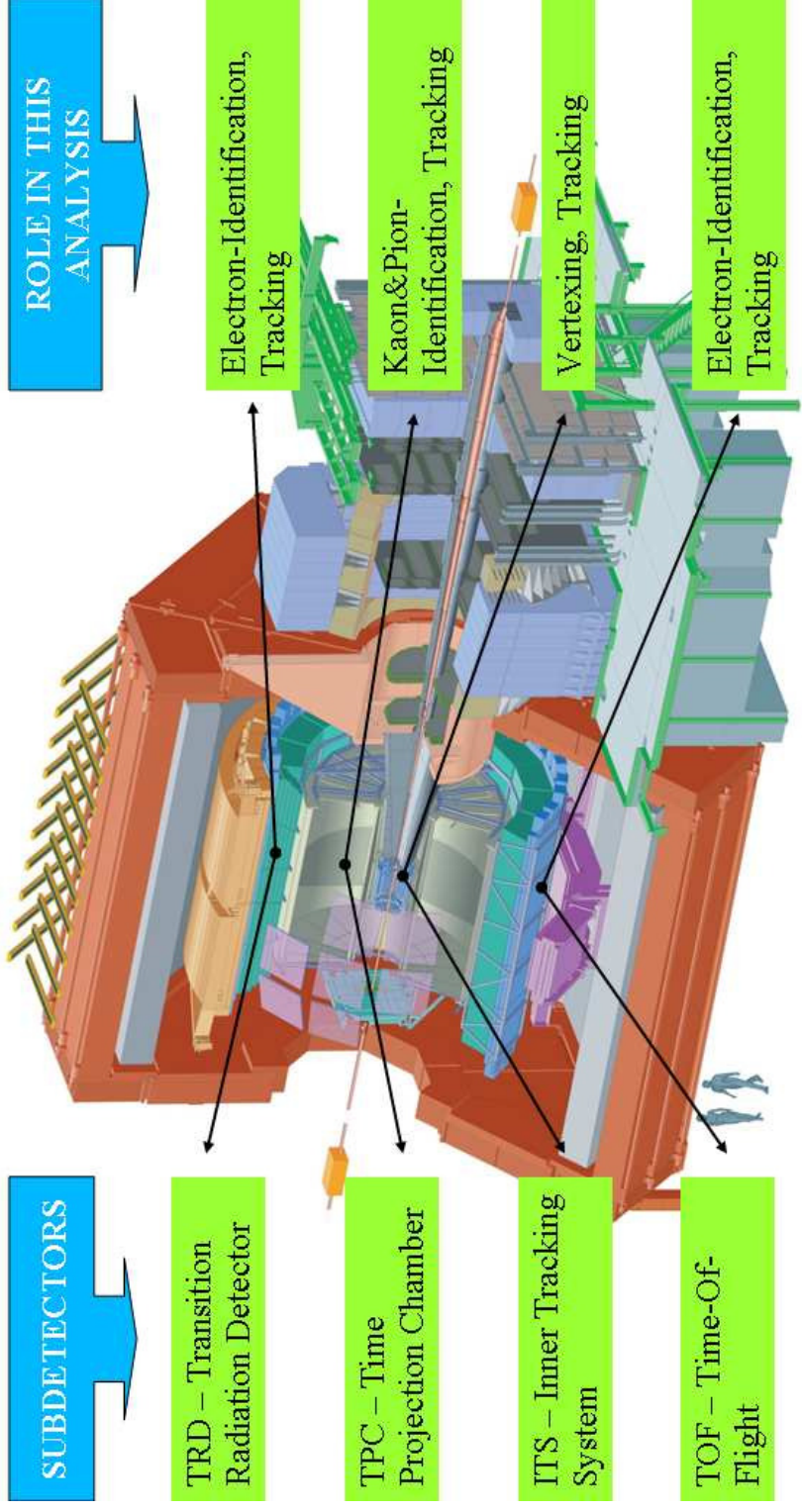


Figure 2.2: The ALICE setup consists of two main parts: central barrel (left red magnet) and the muon arm (blue at right). ALICE has a diameter of approximately 16 meters and a length of 25m (The Zero-Degree Calorimeter (ZDC) is in both directions located at 116 meters from the interaction point). Subdetectors, majorly used in the analysis here, are indicated.

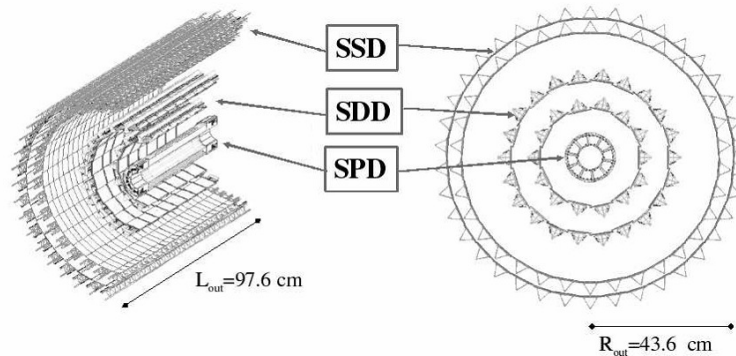


Figure 2.3: Two views of the ITS with its 3 double layer detectors. It is approximately 1 m long and has a radius of about 45 cm ([Col08b]).

range of $|\eta| \leq 0.9$.

For the analysis in the central barrel another parameter which plays a role for low momentum decays, is the magnetic field, which is 0.5 T. The magnetic field points along the beam axis and is generated by a huge magnet, which is housing all central barrel subdetectors.

According to the ALICE coordinate system, z is the direction along the beam axis and r, ϕ are spanning the plane perpendicular to the beam axis.

Subdetectors, playing a major role in the analysis, are described in the following:

ITS Inner Tracking System. The ITS is the first detector system, which detects particles, coming from the collision vertex. It is surrounding the beam pipe and consists of 3 double layers of different type of detectors. These are, starting from the vertex: Silicon Pixel Detector (SPD), Silicon Drift Detector (SDD) and Silicon Strip Detector (SSD), see Figure 2.3. The radius of the SPD is designed such that it has a minimum possible distance to the beam pipe (radius 3.9 cm), for having a very good resolution for primary and secondary vertices and on the outer side the SSD is as close as possible to the TPC (radius 43.4 cm), in order to assure best track matching. The SPD enables the ITS to manage an transverse impact parameter (Closest distance of track to collision vertex in the r, ϕ plane) resolution of roughly $70 \mu\text{m}$ for 1 GeV/c momentum particles (see Figure 2.4). The two track resolution in the r, ϕ plane of $100 \mu\text{m}$ [Col04] is important for checking the distance of two tracks, in order to look, whether they belong to the same mother particle. The provided precision, empowers to select tracks kinematically, in order to reconstruct heavy-flavored mesons, which are a fundament of the analysis here. Since the momentum resolution at low p_t is influenced by

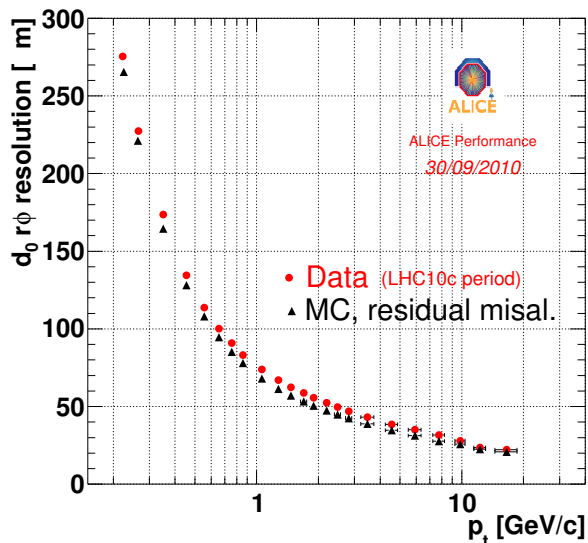


Figure 2.4: Transverse impact parameter resolution as a function of transverse momentum. The distribution is obtained by selecting tracks, which pass general track quality criteria, explained in chapter 5 and create signals in the SPD layers. [Phya]

multiple scattering, the SPD has a design with a very low material budget, which has as result, a radiation length of 1 % per layer. The second and the third detector layers of the ITS (SDD & SSD) are capable to give energy loss information and contribute therefore to the particle identification but are not used in that purpose in this analysis. The pseudorapidity range covered is different for each detector layer and has a minimum of ± 0.9 with the SPD.

TPC Time Projection Chamber. The TPC is the main tracking component in the central barrel. It delivers essential momentum information in a transverse momentum range of three orders of magnitude, starting from around $100 \text{ MeV}/c$ up to $\sim 100 \text{ GeV}/c$. This biggest ever built TPC, provides a huge gas volume, which gives ALICE capabilities especially in the low p_t region. Moreover, it provides in combination with the energy loss information, particle identification. The Kaon and Pion identification which is necessary especially for the analysis here, is done by the TPC alone and the Electron identification on combination with the TOF.

The TPC has pseudorapidity coverage of ± 0.9 for full track length, meaning the track enters through the inner cylinder and reaches at least the outer cylinder of the TPC. For a third of the full track length it extends to ± 1.5 .

The TPC is designed for 8000 charged particles per pseudorapidity unit and per event at a collision rate of 200 Hz in lead-lead collisions. For proton-proton collisions the TPC is designed for a 5 times higher rate, which corresponds still to conditions with more than one order of magnitude lower occupancy, compared to the lead-lead case.

As sketched in Figure 2.2, the TPC has a hollow cylindrical shape with a central electrode at the center and multi-wire proportional readout chambers as end caps. The dimensions of the active volume are: 5 m length, 85 cm inner radius and 250 cm outer radius. The mentioned active volume accommodates 90 m³, which is filled with a gas mixture of $Ne/CO_2/N_2$ in a 90/10/5 ratio [Col08b].

The working principle of the TPC is sketched in Figure 2.5 and described in the following: Particles traversing the gas volume, interact with the filled gas by ionizing the atoms along its path through the detector. As a result of the applied electrical field between the central electrode and the end caps, the released electrons drift towards the pad planes, which are part of detector chambers in the end caps and are segmented in total for all chambers in roughly 560.000 pads. The three-dimensional track is reconstructed by taking the $r\phi$ information from the pad positions with an induced signal and the z coordinate from the drift time. There are three wire planes before reaching the pad plane. Since the number of electrons is not sufficient for creating a measurable signal, they have to be amplified. This is happening in the amplification region, which is separated by the cathode wire plane. The voltages of the cathode wires and anode wires are set in such a way, that electrons drift until the cathode wire plane and are amplified by a created avalanche towards the anode wires. The created positive ions, produced in this process are prevented from drifting into the drift region by the gating grid, since they would cause space charge effects. The measured amount of electrons is proportional to the energy loss of the ionizing particle, as it is the case in proportional counters. Via this energy loss information in combination with the momentum, obtained from the curvature because of the applied magnetic field, particles can be identified according to the Bethe-Bloch formula. The energy loss in the TPC for different type of particles, depending on momentum and the Bethe-Bloch functions for different particle species are shown in Figure 2.6. Particles distributed around the shown curves are assigned to the according particle species. The detailed application of particle identification for the analysis purposes here is explained in section 5.1.

TRD Transition Radiation Detector. The main task of the TRD is to identify elec-

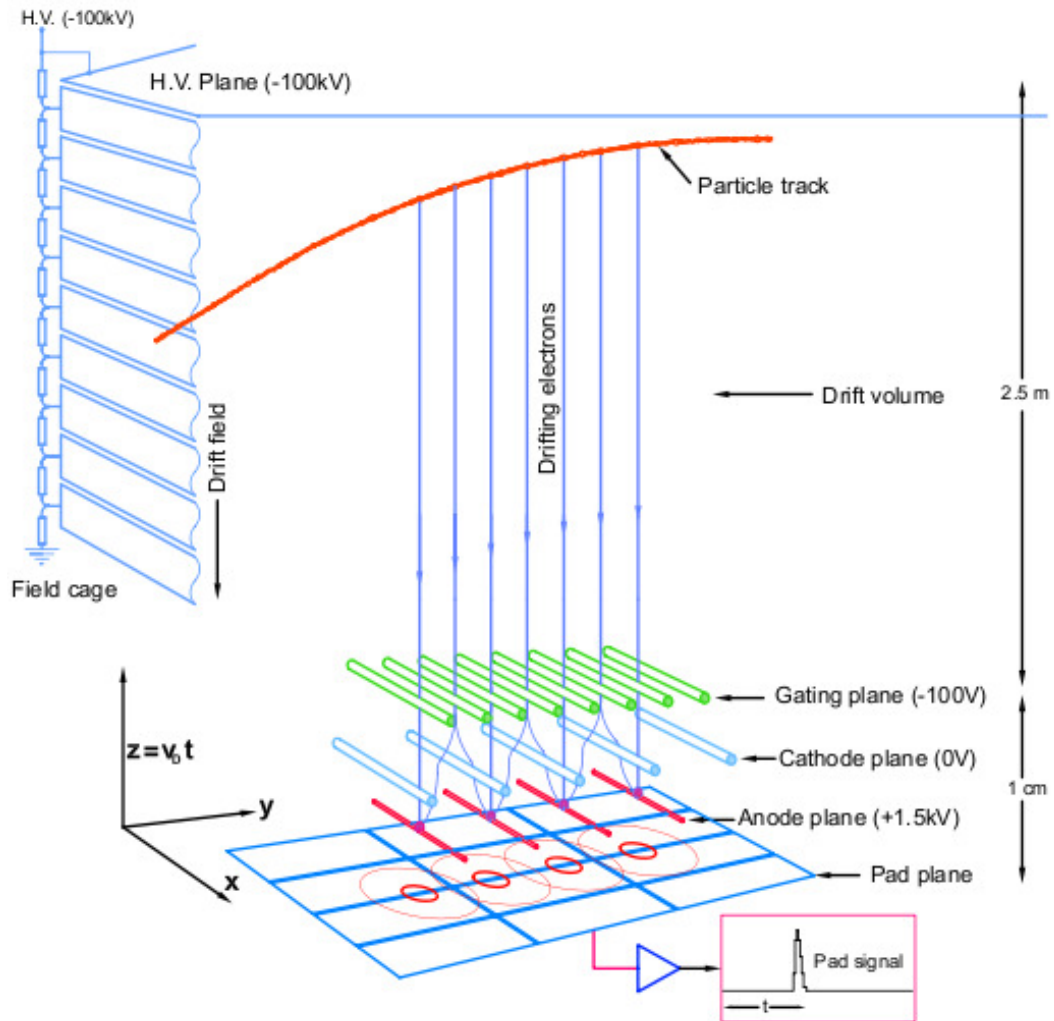


Figure 2.5: Schematic working principle of the Time Projection Chamber (TPC).

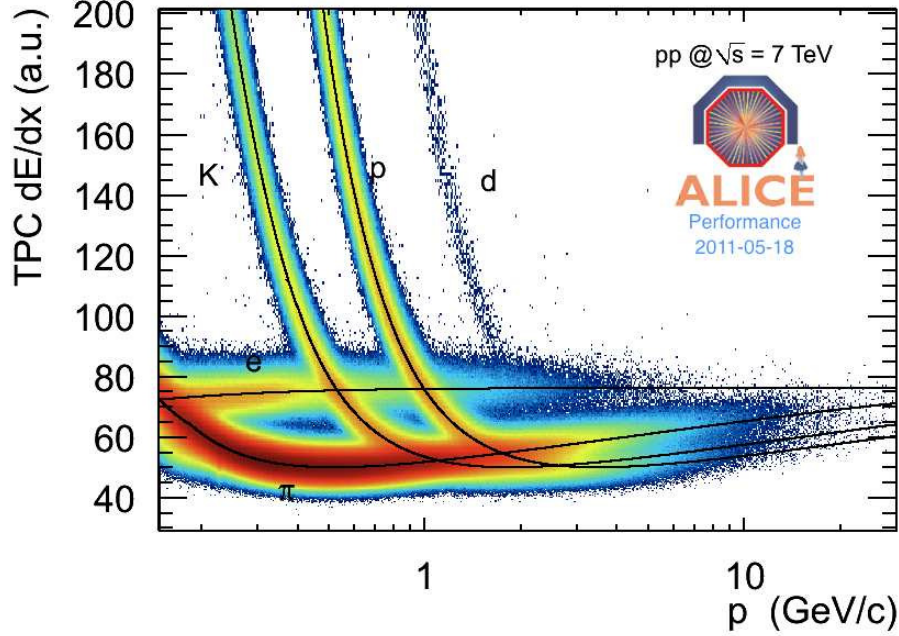


Figure 2.6: dE/dx as a function of momentum of particles traversing the TPC and Bethe-Bloch functions for different particle species [Colb].

trons above 1 GeV/c. At the mentioned momentum region, electrons emit, because of their high Lorentz factor, significantly more Transition Radiation compared to hadrons, while traversing materials with different dielectrical properties [Dol92]. This property is used to separate electrons. Especially the rejection of pions which are abundantly present at such collisions, is through this method possible. The identification of electrons coming from decays of charm and beauty hadrons, plays a fundamental role in the analysis here (chapter 4). The calibration of the TRD is ongoing and the provided particle identification will be used immediately, when it is available, since the electron identification in the mentioned momentum range plays a particular role for the analysis here. In addition, the TRD provides a trigger for high momentum electrons and contributes also to the global tracking.

The TRD is arranged in 18 supermodules along the beam axis with 5 stacks of 6 chambers, which are surrounding the TPC (Figure 2.2). Currently only 10 out of 18 supermodules are installed. Each single TRD chamber has a radiator in front of a multi-wire proportional chamber. The covered pseudorapidity range is ± 0.84 . The length of the complete TRD is 7.8 m and the inner and outer radius are respectively, 290 cm and 368 cm. The TRD has a gas volume of roughly $27 m^3$ and is operated with a Xe/CO_2 (85/15)

mixture.

TOF Time-Of-Flight. The TOF detector provides essential particle identification in the intermediate momentum range (see Figure 2.7). For the analysis here the TOF detector is used for electron identification. Particles are identified by their flight time from the collision vertex up to the TOF detector, since for a given momentum, particles travel shorter or longer time, depending on their mass. Therefore the time resolution is a crucial aspect, which is better than about 40 ps for the ALICE TOF. The technology the TOF detector is based on are Multi-gap Resistive-Plate Chambers (MRPC). The very short gas gaps between layers of electrodes (250 μm), which particles are passing through, are the reason for being a gaseous detector practically without drift time and consequently being very fast.

The MRPC's are arranged in 18 supermodules, containing 5 modules with between 15 and 19 MRPC strips. The TOF detector covers with an active length of 741 cm a pseudorapidity range of $|\eta| \leq 0.9$. Including the outer shell, the TOF detector has an internal radius of 370 cm and an external radius of 399 cm and covers the full azimuth, surrounding the TRD. The total gas volume of 17 m^3 is filled with a $C_2H_2F_4$ (90%), $i - C_4H_{10}$ (5%), SF_6 (5%) mixture.

Figure 2.7 shows the momentum dependent particle separation power of the individual subdetectors of ALICE. The detectors indicated there are: **ITS** - Inner Tracking System, **TPC** - Time Projection Chamber, **TRD** - Transition Radiation Detector, **TOF** - Time Of Flight, **HMPID** - High Momentum Particle Identification Detector, **PHOS** - PHOton Spectrometer, **MUON** - Muon Spectrometer. Except for the first four ones (due to their relevance to the analysis), the latter subdetectors are not described here in more detail. Further information is available in [Col04].

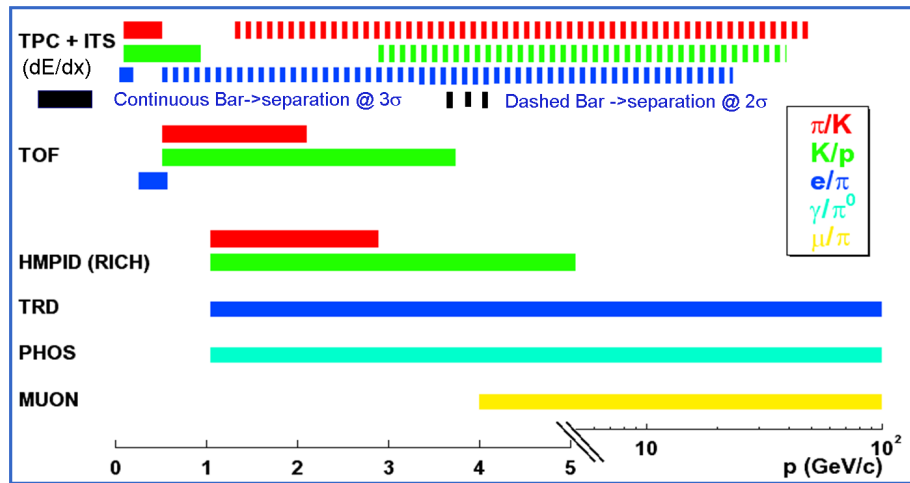


Figure 2.7: Particle separation power for individual detectors as a function of momentum.

Chapter 3

Theory and Motivation of Angular Correlations

An essential way to understand properties of matter is to study the energy loss of particles traversing it. To understand partonic matter a suitable probe for this purpose are heavy quarks, which can sound the created Quark-Gluon Plasma. The energy loss of light quarks is of interest as well and it is obviously interesting to compare the light and heavy quark behavior. Such investigations can be performed for instance by measuring yields and ratios of hadronized particles. For heavy/light quark energy loss comparison D/π ratios are used for example.

An important effect of the heavier mass is, that they have to be created earlier than the light ones, because of the higher energy needed. It should be noted that, the minimum energy necessary, is the double mass of charm or beauty quarks, since quarks are created always as pairs because of flavor conservation. The early creation of heavy quarks, enables them to experience the full space-time evolution of the collision and consequently carries along important information about the Quark-Gluon Plasma. In addition, heavy quarks have the property, that their mass has no contribution from the QCD vacuum and consequently is maintained also in the partonic medium.

In nucleus-nucleus collisions both processes occur: The production and the energy loss of heavy quarks in the created medium. In proton-proton collisions only the first occurs. Therefore pp collisions have the property of being the reference for nucleus-nucleus collisions. As explained in section 1.1, yields of pp collisions are scaled to NN collisions and deviations like suppression of certain particles can be explained by partonic energy loss models, which deliver for example information about the interaction of heavy quarks with the medium. Observing the electron yields originating from heavy flavor, is an example for investigation of energy loss behavior. A distinction among such electrons from heavy-flavor hadron decays (which are called in this thesis shortly heavy-flavor electrons), whether

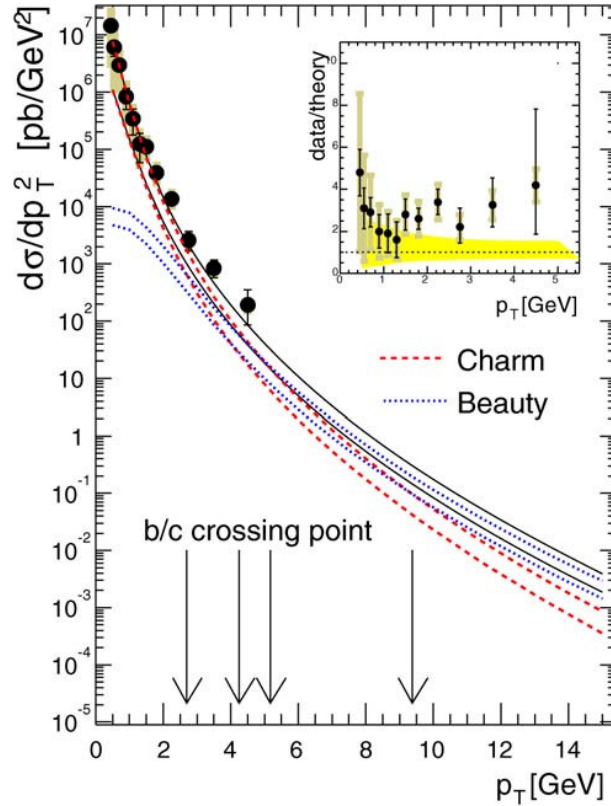


Figure 3.1: PHENIX single electron spectrum in 200 GeV center-of-mass pp collisions [Aea06] and FONLL calculations [CNV05], [ACD⁺06]. Bands in red and blue indicate theoretical uncertainties for the charm and beauty case respectively. In the small box the data/theory ratio is visible.

they originate from charm or beauty quarks is an important information for partonic energy loss models, as it will be seen in section 3.1. For this purpose, a precondition is to distinguish in pp collisions the ratio of charm and beauty quarks from which the electrons originate. As it can be seen in Figure 3.1, according to FONLL (Fixed-Order-Next-to-Leading-Log) calculations for 200 GeV pp collisions, there is a wide p_t range of uncertainty where the cross section of beauty can exceed the charm cross section (2,5 GeV/c - 9,5 GeV/c) [ACD⁺06]. The separation of the mentioned two heavy flavors can be done with Electron- D^0 Correlations. With this method, explained in chapter 4, not only a ratio of charm and beauty cross sections is obtainable, moreover angular properties of heavy-flavor production processes can be studied.

3.1 Partonic Energy Loss

The main energy loss of partons in the medium, created in nucleus-nucleus collisions, is due to multiple scattering and gluon bremsstrahlung. According to the BDMPS model [BDM⁺97], the energy distribution of the radiated gluons is:

$$\omega \frac{dI}{d\omega} \simeq \frac{2\alpha_s C_R}{\pi} \sqrt{\frac{\hat{q} L^2}{4\omega}} \quad (3.1)$$

where the variables are:

- ω , Energy of radiated gluon
- I , Intensity
- α_s , Strong coupling constant
- C_R , Casimir coupling factor, which is 4/3 for quarks and 3 for gluons
- \hat{q} , Medium transport coefficient
- L , Path length in medium

The transport coefficient \hat{q} is defined as the transferred average momentum squared per unit path length ($\langle k_t^2 \rangle / \lambda$) [SW03]. The denominator in the square root in Eq. 3.1 comes from the characteristic gluon radiation, which equals $\omega_c = \hat{q} L^2 / 2$ and is a scale of the energy loss. Eq. 3.1 is valid for $\omega \ll \omega_c$. The average energy loss can then be obtained, by integrating the gluon energy spectrum from 0 to ω_c :

$$\langle \Delta E \rangle = \int_0^{\omega_c} \omega \frac{dI}{d\omega} d\omega \propto \alpha_s C_R \omega_c \propto \alpha_s C_R \hat{q} L^2 \quad (3.2)$$

The energy loss distribution in Eq. 3.1 is obtained by Brownian-like motion through the medium and summing up the interactions with encountered *scattering points*. Because of different relativistic kinematics, for heavy quarks additional considerations have to be done. Due to the lower relativistic β , the radiation inside a cone with a certain angle in moving direction is suppressed, which is called the dead cone effect [DKT91]. Consequently, heavier quarks are assumed to lose less energy [DK01]. Therefore an additional term is applied to Eq. 3.1:

$$\left| \omega \frac{dI}{d\omega} \right|_{Heavy\ Quark} = \left[1 + \left(\frac{m}{E} \right) \sqrt{\frac{\omega^3}{\hat{q}}} \right]^{-2} \frac{2\alpha_s C_R}{\pi} \sqrt{\frac{\hat{q} L^2}{4\omega}} \quad (3.3)$$

E and m are the energy and the mass of the probing heavy quark. As visible in Eq. 3.3, it is expected, that the mass of the heavy quarks plays a fundamental role, in the partonic energy loss physics. A differentiation of charm and beauty quarks, has therefore the potential to clarify the impact of the dead cone effect and partonic energy loss in general.

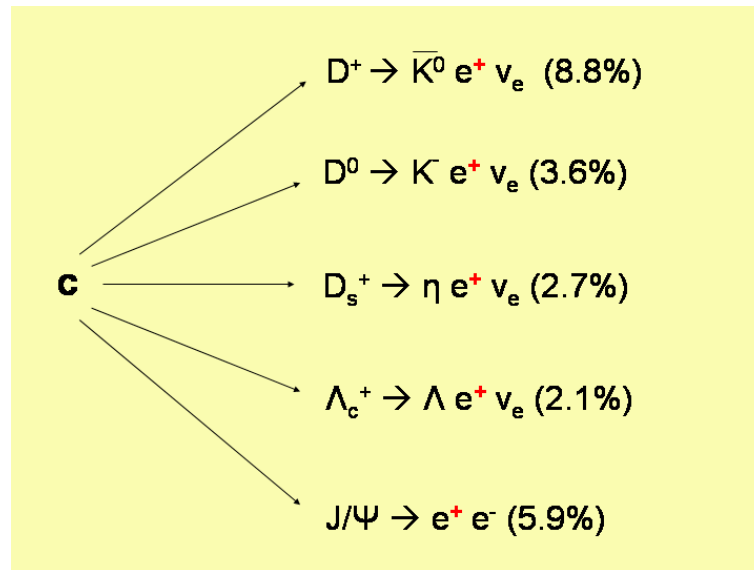


Figure 3.2: Parity relation of the c quark and decay electrons.

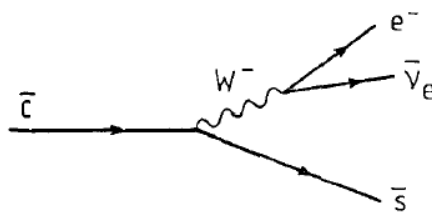


Figure 3.3: Charm quark changes flavor to strange under the emission of a W^- boson, which decays subsequently into an electron neutrino pair. [Bea81]

3.2 Quark-Fragment Parity Inheritance

Produced quarks in nuclear collisions, combine with other quarks, hadronize and decay subsequently. There is a relation between the charge parity of the source quark and the charge parity of its fragments. For instance, the charm quark, goes in its decay stem, most abundantly to a positron and not to an electron. Similarly the anticharm ends predominantly with electrons. For the bottom quark there are predominantly electrons among the fragments and vice versa for antibottom. The decay chains, starting from the c quark for example, are depicted in Figure 3.2 (For the \bar{c} case, the antiparticles are the outcome). The reason for the mentioned parity relation is the quark state transition pattern of the decay mode illustrated in Figure 3.3. Since the electrical charge of the \bar{c} quark is $-2/3$ and the \bar{s} quark is

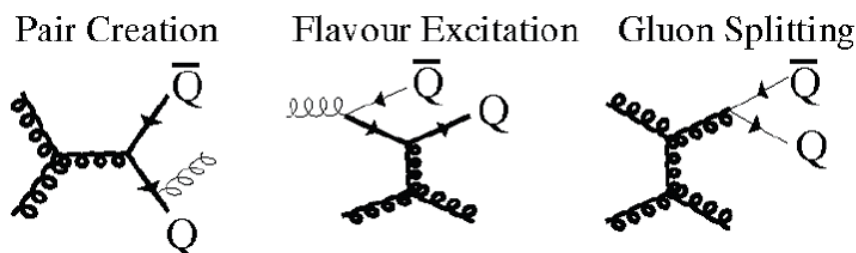


Figure 3.4: Main production processes of heavy flavor [Col06a].

$+1/3$, because of charge conservation, the flavor change occurs via an W^- boson. If the \bar{c} is a quark of D^0 and the \bar{s} of a K^+ , this change of quark flavor represents the reaction $\bar{D}^0 \rightarrow K^+ e^- \bar{\nu}$.

The shown meson and baryon products in Figure 3.2 cover almost hundred percent of charm, produced in the collisions. Furthermore exemplified major semileptonic decays display the dominant abundance of positrons compared to electrons. In order to quantify this fact with additional other features, the expression Parity Inheritance Factor, shortly PIF is introduced. $PIF(c \rightarrow e^-, [P]) = a$ means, the statistical fraction of c going to electron for a certain momentum bin is a . Experiment specific conditions like for example reconstruction efficiencies, background suppression applications and coverage can be included in the PIF, all emblemized with a diamond: $PIF(c \rightarrow e^-, \diamond, [P]) = a$. The PIF values are obtained by simulations, which incorporate correct branching ratios, direct and indirect CP violation effects and moreover experiment specific constraints (see Appendix B). The role of PIF's in this analysis is explained in Chapter 4.

3.3 Topology of Leading Order Processes

The production of heavy flavor in nuclear collisions can be categorized by three leading order processes. These are pair creation, flavor excitation and gluon splitting. The corresponding Feynman diagrams with additional parton shower processes (thin lines) as they are also implemented in the PYTHIA event generator¹ are shown in Figure 3.4.

In the pair creation process, two partons from colliding two different protons interact and create a new $q\bar{q}$ pair. In the case of flavor excitation the produced $q\bar{q}$ pair originates from the same proton, where one of them is scattered by a third

¹PYTHIA is an event generator program for high energy physics [SAC⁺]. It contains a number of physics aspects but is only exact at leading order. All simulations, shown in this thesis, are done with PYTHIA 6 for $\sqrt{s}=7$ TeV pp collisions, if not another simulation is explicitly mentioned.

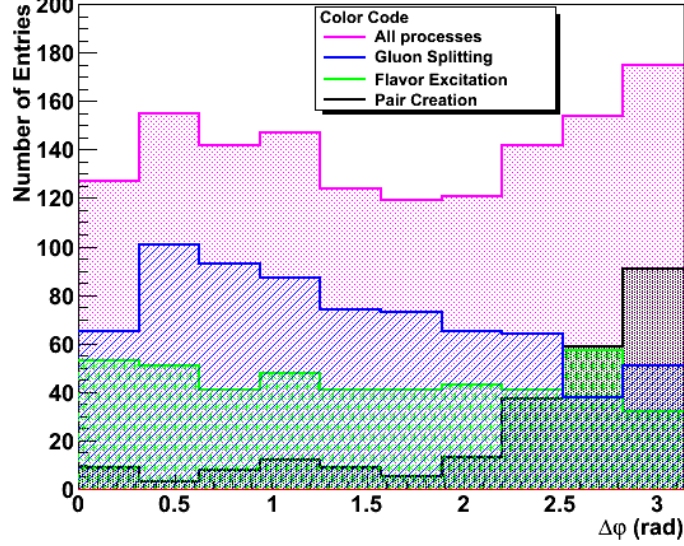


Figure 3.5: Angular distributions of single production processes for $c\bar{c}$ pairs in $\sqrt{s}=7$ TeV pp collisions obtained from PYTHIA. The angular correlation is performed in the plane perpendicular to the beam axis, in which the azimuthal angle φ is defined between the q and \bar{q} directions of flight.

parton. It should be noted, that if the created pair is for example $c\bar{c}$, the initial state pair is also a $c\bar{c}$ pair, being already present in the structure function of the proton. For the gluon splitting process on the contrary, there is no heavy-flavor quark participating in the hard scattering process. Heavy quarks are created in this type of process later in the splitting of an outgoing gluon.

Depending on the process type, the outgoing heavy quarks are due to momentum conservation correlated in flight directions. For pair creation there is a back-to-back, for gluon splitting a same side orientation. Flavor excitation has also the same side orientation but is less pronounced. The angular properties of the single processes for $c\bar{c}$ pairs in $\sqrt{s}=7$ TeV pp collisions obtained from PYTHIA can be seen in Figure 3.5.

3.4 Correlations in η - φ Space

Usually, as it is the case in the analysis here, correlation studies are performed in the perpendicular plane to the beam axis. In this section a short excursion is done in order to give an impression about the possibility to make the correlation analysis in 3 dimensions, instead of taking the φ angle as reference. Since the correlation

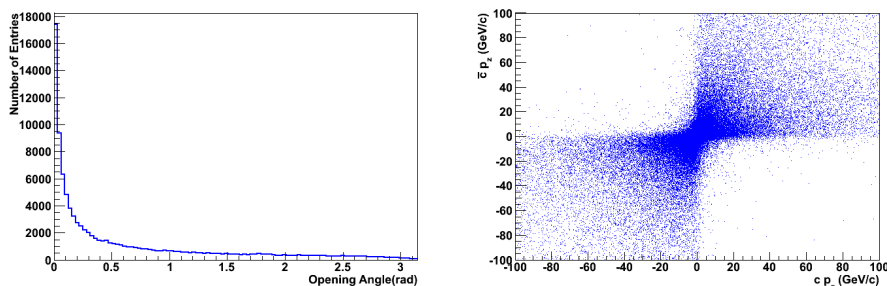


Figure 3.6: Left: Narrow real angle (opening angle) in full space between the produced charm and anti-charm quarks, due to the relativistic boost in their production at LHC energies. Right: Longitudinal momentum relation of $c\bar{c}$ pairs.

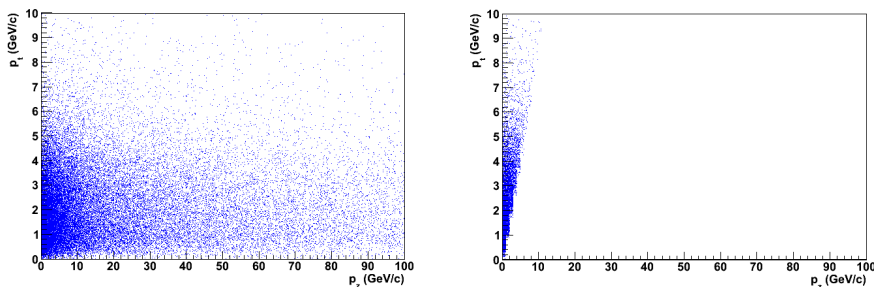


Figure 3.7: Left: Transverse and longitudinal momentum relation for c quarks. Right: Same like left but at mid-rapidity ($|\eta| < 1$).

in phi is a projection of the real angle in 3 dimensions, one may think about to take the real angle, in order to get a more accurate correlation. The result of simply taking the real angle between the $c\bar{c}$ pair is shown in Figure 3.6. The reason for the predominantly narrow angles are the ultrarelativistic conditions at LHC, which cause very big Lorentz boosts. Even there is a symmetric momentum of the colliding protons, the partons in the proton frame have a momentum distribution. As a consequence the $c\bar{c}$ pairs have in the lab frame seldom a net momentum close to zero. As shown in Figure 3.6, the $c\bar{c}$ pair has almost always the same p_z sign, which means, that they fly together in z or $-z$ direction (The z -direction is in the ALICE coordinate system parallel to the beam axis). Moreover the momentum components in z -direction (p_z) are much bigger than the components in the transverse direction (p_t). This contributes also essentially to the closeness of the flight directions in the real angle. The relation of p_z and p_t of the same charm quark are shown in Figure 3.7. On the other hand, doing analysis in the central barrel of the experiment, at mid-rapidity, restricts naturally big p_z values, because

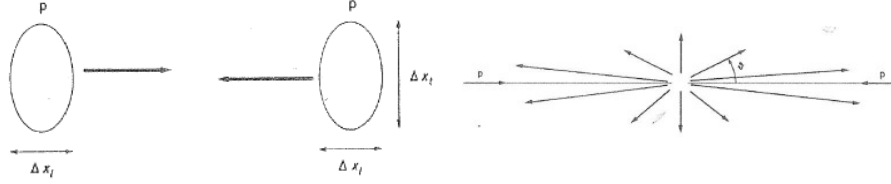


Figure 3.8: Left: Incoming protons at relativistic energies. Right: Relation transverse vs longitudinal momentum of outgoing collision products.[Nac86]

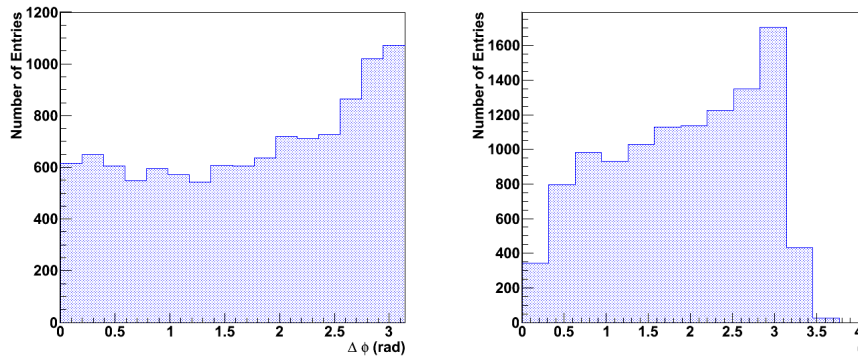


Figure 3.9: Angular Correlation for $c\bar{c}$ pairs in $\Delta\varphi$ and in d variable.

of the limited coverage in η (see Figure 3.7). The bigger p_z values originate from the Uncertainty Principle. Since the protons are longitudinally Lorentz contracted but not in the transverse direction, a greater uncertainty for the transverse momentum arises (see sketch in Figure 3.8). The mean momentum in the transverse and in the longitudinal are coupled via the uncertainty relation. For relativistic collisions consequently a momentum distribution of outgoing particles, as sketched in Figure 3.8 occurs. Under the described conditions it is important to have a definition of an appropriate angle. Since the p_z values differ by order of magnitude it is inconvenient to take in the mentioned boost conditions simply the opening angle. For correlation purposes the distance d , which is defined in the $\eta - \varphi$ space could be used. This variable is used for example in Jet physics in order to define a Jet cone. Here it should be used to express closeness under boost conditions. The distance d is calculated such: $d = \sqrt{(\eta_2 - \eta_1)^2 - (\phi_2 - \phi_1)^2}$. The handicap of d is, that it is not infrared safe but since η is restricted, the infrared safety is given. In Figure 3.9 and 3.10 angular distributions in d and in φ for charm and beauty quarks, being both within $|\eta| < 1$, are shown as example. As seen there, an improvement due to the distinction with the d variable, in the sense of having clearer and better separable structures, is not clearly recognizable. This is not unexpected,

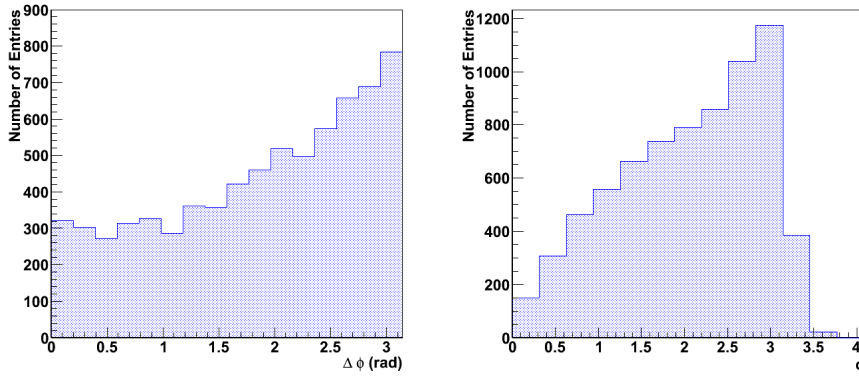


Figure 3.10: Angular Correlations for $b\bar{b}$ pairs in $\Delta\varphi$ and d variable.

since at LHC energies, where particle distributions span almost over 10 units of rapidity, doing analysis in the central barrel means, restricting big p_z values. A restriction of p_z values, implies the approaching of transverse momenta to global momenta and as a result, spatial considerations can be approximated to a certain degree by transverse ones.

Chapter 4

Angular Electron-Hadron Correlation Methods

As explained in chapter 3, the separation of charm and beauty contributions plays an essential role in the measurement of the relative production cross section. The separation can be done on a statistical basis, using angular correlations of electrons and D^0 mesons. For this purpose there are already two methods, employed in former experiments and in the literature and a new one is introduced as part of this thesis, all three described in the next sections. In all three methods the analysis is performed using the fragmentation products in the two *arms* originating from the initially created heavy quark pair (see Figure 4.3 as an example illustration).

4.1 Shape Fitting Method

As mentioned above, the created heavy-quark pair fragments into two arms of particles. In this method, after measuring the angular distribution of D^0 mesons relative to heavy flavor electrons, originating from the two mentioned particle arms, the separation is done, based on the fact that B meson and D meson decays have different Q values. As a consequence of the different energy releases, the B meson daughters have a bigger transverse momentum relative to the flight direction of the mother particle. Therefore electrons and D^0 mesons coming from B meson decays lead to a wider angular distribution. That the decay chain of B mesons contains more sequences, contributes also to the width of the distribution. The result is obtained by fitting the full shape of the correlation function with PYTHIA, leaving the charm to beauty ratio free. The same method can also be applied to electron-hadron correlations, by correlating heavy flavor electrons with charged hadrons. The application of such fits can be seen in Figure 4.1. The drawback of the shape fitting method is, that it has an essential model dependency. As

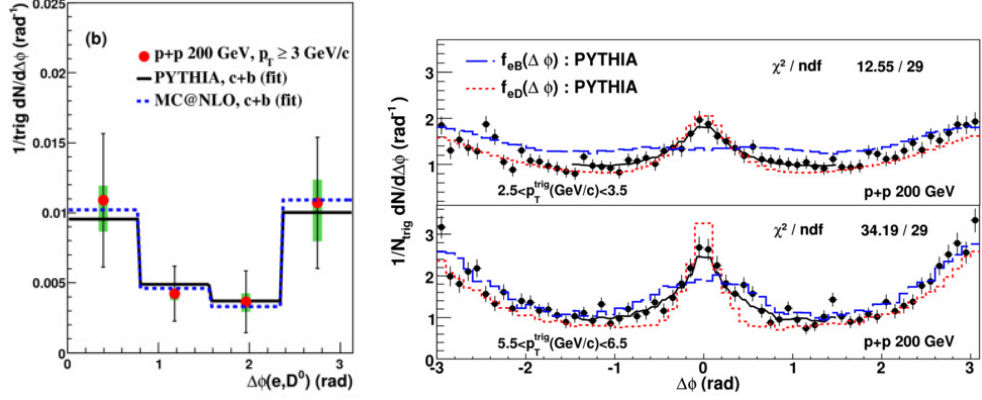


Figure 4.1: Correlations measured at STAR [Aea10]. Left: Electron- D^0 correlations. The fit shapes are shown with solid and dashed lines for different simulations. Right: Electron-hadron correlations for two different electron transverse momentum ranges. The simulation fit shape is indicated by dotted and dashed curves for D and B meson decays. The solid curve is the total fit .

an example, the angular distributions of charm and beauty quark pairs obtained from MNR code¹ [MNR92], in Figure 4.2, shows different behavior, especially in back to back correlations (see for comparison Table B.1 and Figure 3.9 and 3.10 obtained from PYTHIA, which is only exact at leading order, as mentioned before).

4.2 Angular Separation by Charge Sign Condition Method

This method of separation is introduced at the STAR experiment at RHIC [Mis09], [MftSC08]. The idea of kaon-pion charge sign tagging method was already employed for investigation of $D^0 \bar{D}$ production at ²ISR [Bea81]. The analysis is based majorly on two physical characteristics: One are the angular properties of the underlying QCD processes -see section 3.3- and the other is the charge relation of quarks and their fragmentation products as described in section 3.2. As sketched in Figure 4.3, taking the electron as reference, K^- coming from D^0 is for charm preferentially on the away-side and for beauty on the near-side. As a

¹MNR is a simulation program based on perturbative QCD at Next-to-Leading Order (NLO) precision. It provides only inclusive distributions.

²Intersecting Storage Rings

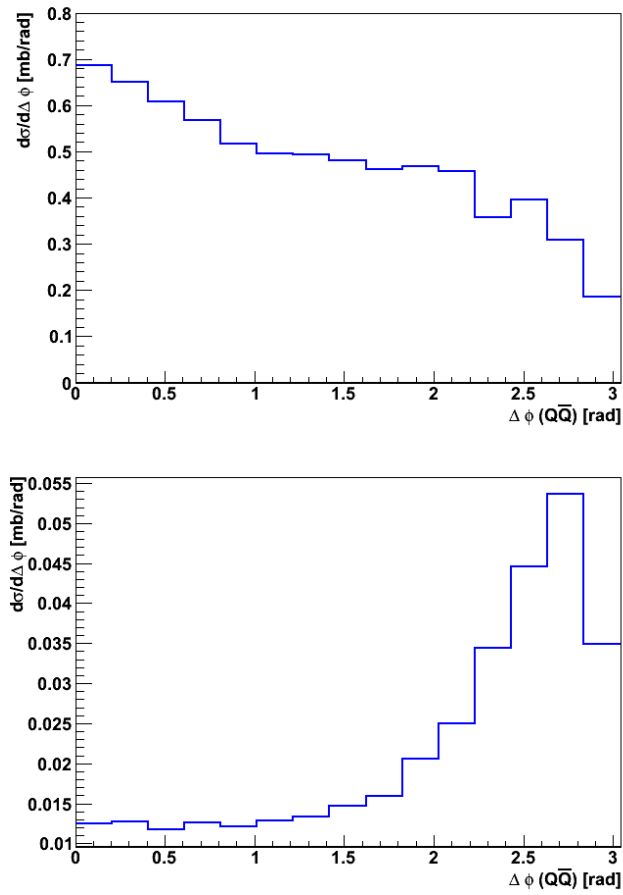


Figure 4.2: Azimuthal distribution of $c\bar{c}$ pairs (top) and $b\bar{b}$ pairs (bottom) within $|\eta| < 1$, created in 7 TeV pp collisions. Calculation from [MNR], using [MNR92]. Compare with Figure 3.5 for the $c\bar{c}$ case.

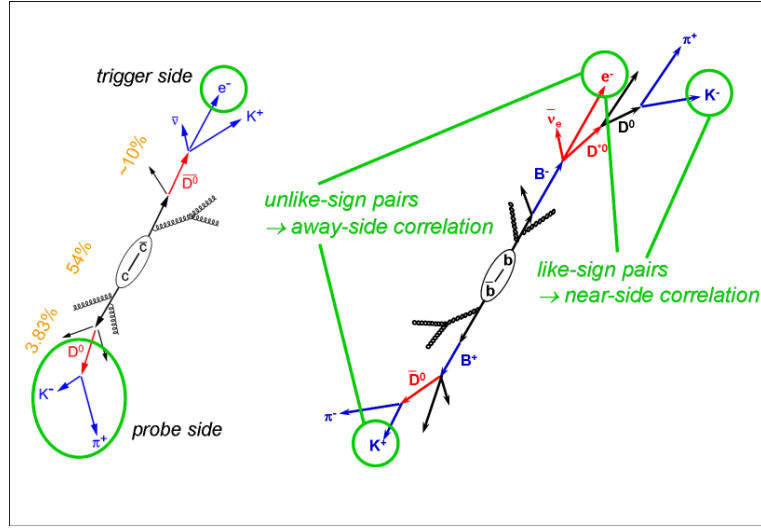
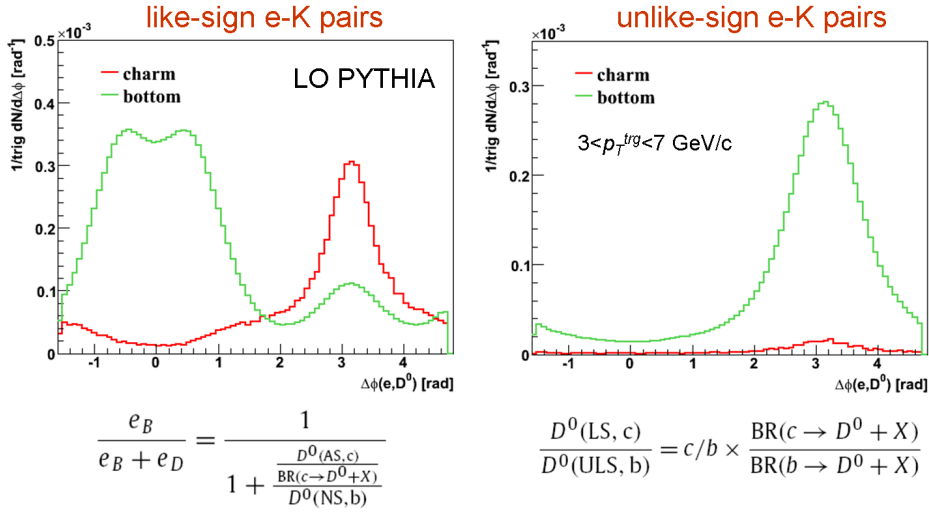


Figure 4.3: Illustration of decay topology of example charm and beauty quark fragmentation. The like-sign electron-kaon pair is for the charm case back to back oriented and for the beauty case same side oriented. The Unlike-sign electron-kaon pair exists only in the beauty case and is back to back oriented (If CP violation and oscillation effects are neglected).

consequence, if one looks to the accordingly simulated distribution (Figure 4.4), a separation at $\pm \frac{\pi}{2}$ ($\pm \approx 1.57$ rad in the figure) delivers on the near-side the beauty contribution and on the away-side the charm contribution. Correlating electrons with K^+ , yields only beauty contribution. Since the \bar{c} quark fragments either to electrons or to \bar{D}^0 , a coexistence is almost excluded. By using the formulas below the distributions in Figure 4.4, the charm to beauty ratio can be obtained. The drawback of this method is the assumption of clearly separated angular structures. As already mentioned, the MNR calculation (Figure 4.2), which is next-to-leading-order, shows that each of charm and beauty contributions can yield on near- and on away-side in the angular correlation distribution.

4.3 A New Method: Factorization

The factorization method is similar to the one in section 4.2 and is based on the same arguments. As mentioned, the charge correlation of the final state particles and the parity of the source quarks lead for charm and beauty cases to different characteristic angular distributions. In this method, electrons coming from semileptonic decays of mesons with charm or beauty content, are correlated in angle with D^0 mesons originating from the same hard process. It is realized by



(AS: Away Side. NS: Near Side. LS: Like-Sign. ULS: Unlike-Sign.)

Figure 4.4: Angular distribution simulations and evaluation formulas. Left: Like-sign correlations of electrons and kaons. Right: Unlike-sign correlation of electrons and kaons.

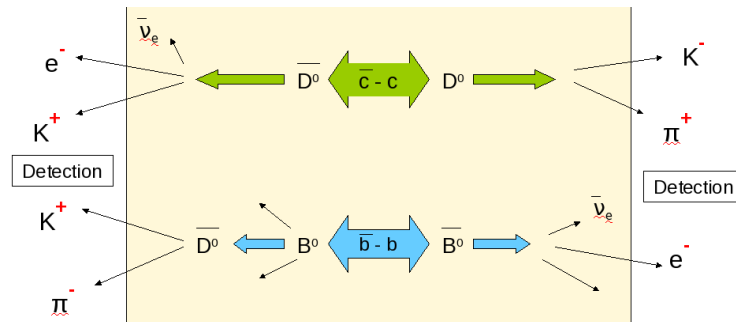


Figure 4.5: Example decay stems for a $c\bar{c}$ and $b\bar{b}$ pair. The charge parity and the orientation of the detected particles, provide the possibility of distinction between charm and beauty production.

listing all possible process combinations, which lead to an occurrence in the correlation distribution. Two example process chains are shown in Figure 4.5. As seen there, a correlation of electrons with \bar{D}^0 for the case of a $c\bar{c}$ pair is not possible (except in the case of CP violation, which is a very small effect for D mesons, as quantified in the following paragraph). A back to back angular correlation of the electron and D^0 occurs in the case of flavor creation as charm production process. A selection of a back to back correlated electron \bar{D}^0 pair would pick a $b\bar{b}$ pair, as depicted lower in the figure. There are more possibilities of fragmentation and decay chains, since charm and beauty hadronize to different hadrons like D^+ , B^+ as well. The fractions of destination hadrons, in which charm and beauty hadronize are shown in Figure 4.6. Electrons are selected from the decay of all hadrons displayed in the figure and are correlated with the most abundant and charm containing hadron, namely D^0 mesons. B mesons decay also richly in D mesons. For instance decays B^+ in its inclusive mode roughly 79 % to \bar{D}^0 [Aea08]. To separate those D^0 mesons originating from B mesons, from the ones originating directly from charm, means to understand the charm to beauty ratio. The combination of the parity (electrical charge sign) of electrons and D^0 mesons with their angular relation, enables to realize the mentioned separation. The contributions coming from such combinations are systematized in the following.

Electrons are taken from all charm and beauty hadrons listed In Figure 4.6 and from the other leg of the created heavy-flavor pair, D^0 mesons are taken. It is possible to deduce from an angular correlation function the relative charm and bottom ratios, by comparing the regions less and greater than $\frac{\pi}{2}$ in the azimuth φ (The azimuthal region $[\pi, 2\pi)$ is mirrored to $[0, \pi)$, where as mentioned before, φ is the azimuthal angle with respect to the beam axis.). The correlations are categorized in two types:

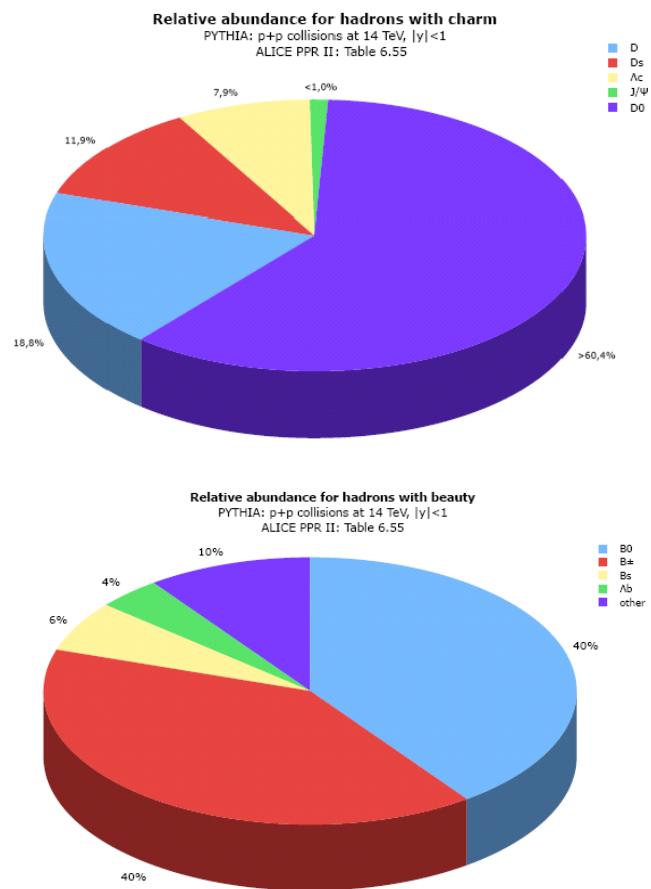


Figure 4.6: Hadron fractions containing charm or beauty quarks [Col06b].

- Correlation Type I: e^-D^0
- Correlation Type II: $e^-\bar{D}^0$

The correlations are obtained by histogramming the D^0 or \bar{D}^0 φ angle relative to the electron, according to the correlation type. Of course symmetric charge conjugated cases are always also considered. The single contributions in different φ regions can be seen in Figure 4.7 and 4.8. Each tagged contribution (numbers

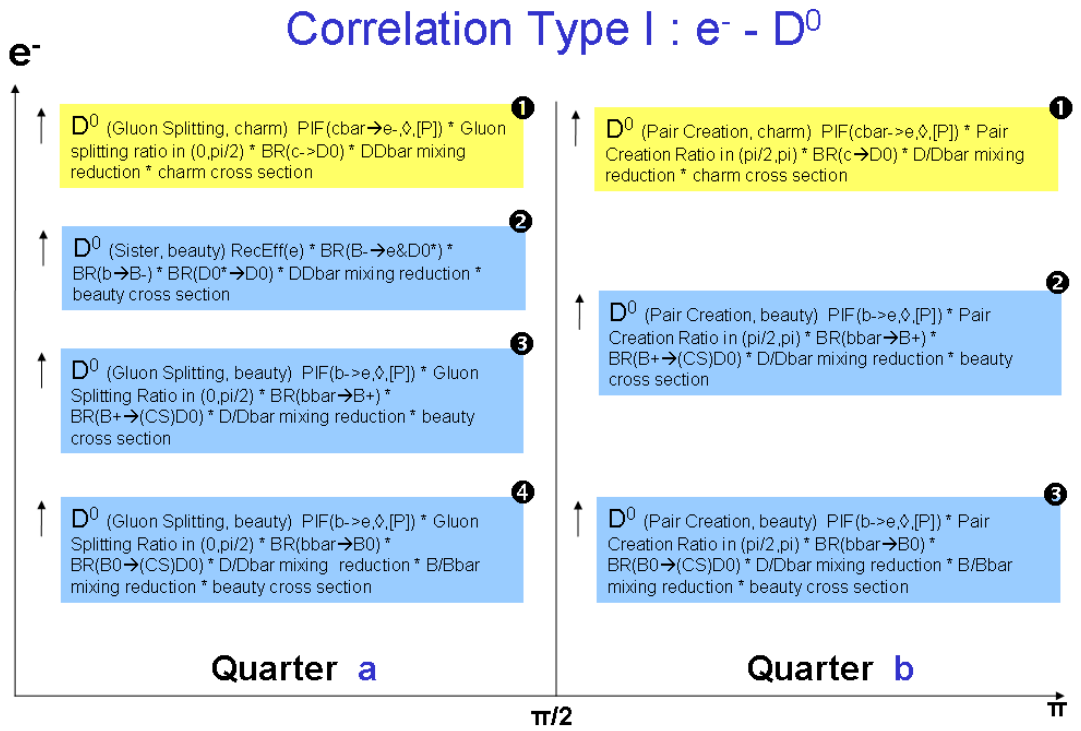


Figure 4.7: Electrons correlated with D^0 mesons. Single contributions to the correlation are listed in quarters of occurrence. Same-side D^0 mesons are in Quarter a and away-side ones in quarter b.

in black circle), represents a combination of processes and the according cross section for this certain process chain. For example, if we take contribution no. 2 in Correlation Type I in quarter a, the factors listed there in the same order are explained in the following:

- The b quark QCD creation process can be any. The electron occurs because it is in company of the D^0 coming from the same decay chain ($B^- \rightarrow e^- \nu_e D^{*0} (\rightarrow D^0 X)$).

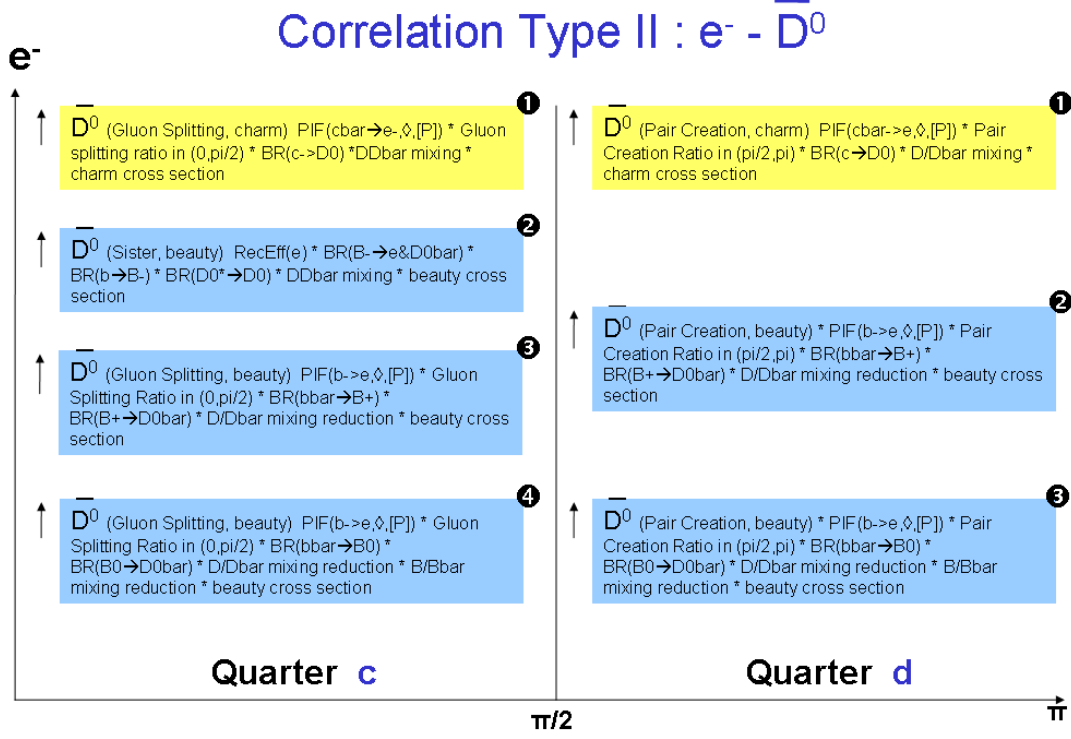


Figure 4.8: Electrons correlated with \bar{D}^0 mesons. Single contributions to the correlation are listed in quarters of occurrence. Same-side \bar{D}^0 mesons are in Quarter c and away-side ones in quarter d.

- ▶ Reconstruction efficiency of accompanying electron
- ▶ Fragmentation ratio (see Figure 4.6)
- ▶ Branching ratio of the mentioned decay mode (The mode $B^- \rightarrow e^- \nu_e D^0$ is also included. Values taken from [Aea08])
- ▶ D^0 mesons at the end of the decay chain can undergo an oscillation process and cause therefore, statistically a reduction of this contribution. D^0/\bar{D}^0 mixing is a small effect, in the order of 0.3% [Col08a] and has therefore not a big impact. For B^0/\bar{B}^0 mixing is much more significant, since it occurs with roughly 19 % [Aea08]. The direct CP violation is already in the branching ratio considered.
- ▶ Beauty cross section

Another example type is contribution tagged with number 1 in quarter d in Correlation Type II:

- ▶ The underlying QCD process responsible for charm production is pair creation.
- ▶ A fraction of \bar{c} goes to electrons (measured by PIF, explained in section 3.2).
- ▶ Fraction of Pair creation processes with away-side ($\frac{\pi}{2} - \pi$) orientation. This value can be obtained from PYTHIA but also from other simulations (see Appendix B).
- ▶ Branching ratio
- ▶ D^0/\bar{D}^0 mixing but this time not the reduction by this process. This contribution is only possible if the oscillation occurs.
- ▶ Charm cross section

An illustration of the formation of an example contribution type is shown in Figure B.1. Beside the listed ones, there are more contributions, which are not listed in Figure 4.7 and 4.8 for overview reasons, in order to avoid repetitions. Gluon splitting contributes also to the back to back correlation and can create also entries in quarter b and d. The same is valid for the flavor excitation process, which is also not shown. The production process types are mentioned here for explanation reasons. In the analysis the sum of angular distributions of all process types are taken and the contributions are not computed for each process type individually. The details of the contributions are of fundamental importance, for the understanding of the underlying processes, since the correlation function shown in Figure 3.5, is on quark&quark ($c\bar{c}$) level, and here the correlation is on leptonic&hadronic (e- D^0) level. On the other hand, if charm and beauty cross sections are taken as ingredients, conclusions on the angular distribution of the QCD production processes can be done. If we take the charm and beauty cross section as unknown, a set of equations can be established. All factors in the mentioned equations are obtained from experimental data or from simulations. As result for each contribution a single number as factor of the cross section can be written. Since in this analysis the aim is to obtain a charm to beauty ratio, variables which cancel are not included (Absolute values of the charm and beauty cross sections can be gotten by multiplying each factor with the D^0 reconstruction efficiency and normalizing the entries in the quarters with the number of events analyzed and the

inelastic cross section.). If the contributions in each quarter are summed up, one obtains:

$$\text{Quarter } a = k_1 * \sigma_{charm} + k_2 * \sigma_{beauty} \quad (4.1)$$

$$\text{Quarter } b = k_3 * \sigma_{charm} + k_4 * \sigma_{beauty} \quad (4.2)$$

$$\text{Quarter } c = k_5 * \sigma_{charm} + k_6 * \sigma_{beauty} \quad (4.3)$$

$$\text{Quarter } d = k_7 * \sigma_{charm} + k_8 * \sigma_{beauty} \quad (4.4)$$

where, taking the MNR angular distribution values, the variables are:

$$k_1 \approx 2.040 * 10^{-3}, k_2 \approx 6.095 * 10^{-3}, k_3 \approx 0.917 * 10^{-3}, k_4 \approx 0.351 * 10^{-3}, \\ k_5 \approx 0.006 * 10^{-3}, k_6 \approx 0.850 * 10^{-3}, k_7 \approx 0.003 * 10^{-3}, k_8 \approx 2.698 * 10^{-3}.$$

For example the factor k_1 is obtained from contribution number 1 in Quarter a and k_2 from the sum of contributions number 2,3 and 4 in the same Quarter in Figure 4.7. All other factors are obtained with the same logic, as described above.

The determination of the yields in the four quarters are the main measurements for this analysis. The set of equations, shown above, is an overdetermined system, since there are more equations, than unknowns. The least square method can be applied here to find a solution for the equation set. The charm to beauty ratio can be computed only with one type of correlation. If both differ too much from each other (no agreement within errors), the comparison delivers an important inconsistency check.

Factorability is only valid if the single processes of a contribution are independent. This is for the majority of the processes the case but there are a few exceptions, which need to be parametrized: The D^0 has a different reconstruction efficiency depending on p_t . The same is valid for electrons. Another dependency on p_t concerns the angular distribution of the underlying QCD processes. These dependencies can be overcome by using the according values, matching the momentum interval.

It should be noted, that b quarks which fragment into c quarks are counted here to c quarks.

The factorization method proposed in this analysis, reduces the model dependency and has the advantage to be able to take the best information at each step, so taking experimental measurements or next-to-leading order informations about angular distributions, as example.

Chapter 5

Angular Correlation Analysis

The ingredients of this analysis are heavy-flavor electrons and D^0 mesons. Therefore the analysis has to start with the reconstruction of D^0 's and the selection of heavy-flavor electrons.

General Features of Analysis

The reconstruction of recorded events is happening in several iterations. The higher the pass number, the better is the quality of the reconstruction, for reasons like improved calibration of the detectors for example. By the time this thesis is written, roughly $244 * 10^6$ pass 2 pp events at 7 TeV were available. In the correlation analysis only pass 2 data are used and thus only a fraction of the recorded events are analyzed.

In order to eliminate background sources like beam-gas interactions, events used in this analysis fulfil certain criteria: To be selected by the bunch crossing trigger, which is provided by LHC detectors and the requirement of at least two hits in the trigger detectors. Moreover a cut in the SPD cluster versus tracklets correlation is applied, which has different trends for beam-beam and beam-gas interactions. More detailed information about the physics event selection is available at [Cola].

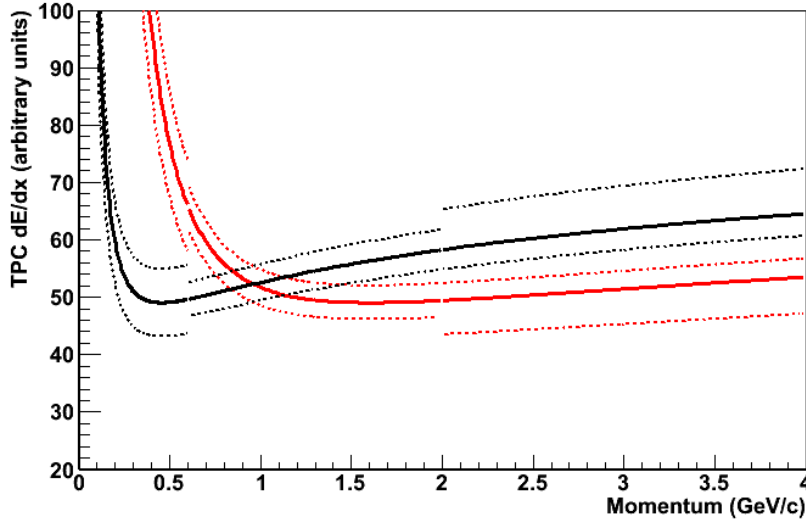
Particle Identification (PID) features of ALICE are essentially contributing to the analysis. For this analysis the detection of three particles are of interest: Kaons, pions and electrons. Kaons and pions are identified by the TPC and the electrons additionally by the TOF, i.e. only central barrel detectors are used. Tracks of all three particles have to fulfil the single track cuts, in order to suppress tracks with bad quality. These conditions are:

- Number of clusters in TPC greater than 50.

- $\chi^2/cluster$ in TPC less than 3.5.
- Values of the diagonal of the covariance matrix less than: 2,2,0.5,0.5,2 for, variance in x, variance in y, variance of curvature in the pad plane projection, variance of $\tan\lambda$ (where λ is the angle between track and pad plane), variance of η (where η is the product of the curvature and x_0 the center of the curvature).
- Requirement of a TPC Refit.
- DCA to vertex in xy plane less than 3 cm.
- DCA to vertex in z less than 5 cm.
- Rejection of tracks with kink.
- Requirement of a ITS Refit.

5.1 D^0 Reconstruction

The D^0 contains a $c\bar{u}$ quark pair and has a mass of $\sim 1865 \text{ MeV}/c^2$. The decay length $c\tau$ is $\sim 123 \mu\text{m}$ [Aea08]. The major challenge in this analysis was the reconstruction of D^0 in the decay mode (Of course \bar{D}^0 with its charge conjugated daughters are also always considered in this section.): $D^0 \rightarrow K^-\pi^+$ 3,89%. For the reconstruction first kaon and pions are identified via their momentum dependent energy loss in the TPC, as explained in Chapter 2. The momentum information is taken from the global track and not only from the TPC. Since the single track cuts require at minimum the TPC and ITS participation in the track reconstruction, the momentum resolution is less than 5% below 10 GeV/c [Otw11]. With the single track cut requirement of minimally 50 clusters, the energy loss resolution is below 10% [A+10]. The energy loss values are scattered around the Bethe-Bloch curves with a gaussian distribution as displayed in Figure 2.6. In order to select the desired particles, a number of sigmas, according to the mentioned gaussian distribution, around the curves are applied. Nevertheless it is unavoidable to get mixing at crossing points of the curves of different particle species. For the identification of kaon pion pairs and minimizing the mixing, the sigmas are adapted as following: The momentum range is subdivided in three parts. In the low and high momentum ranges the sigmas are such applied, that the bands around the Bethe-Bloch curve don't overlap. In the intermediate range both bands are overlapping, because of the crossing of the curves, but are kept narrow. The upper and lower sigmas around the Bethe-Bloch curve are applied asymmetrically, since between the curves of kaon and pion, the mixing is higher.



Momentum Range (GeV/c)	0→0.6	0.6 →2	2→
Upper Kaon Sigma	2.8	1.4	1.4
Lower Kaon Sigma	2.8	1.4	4.2
Upper Pion Sigma	2.8	1.4	4.2
Lower Pion Sigma	2.8	1.4	1.4

Table 5.1: Top: Sketch of momentum dependent subdivisions of applied sigma values. Thick lines are Bethe-Bloch functions and thin lines the adapted sigma cuts. Bottom: Table of TPC dE/dx sigma values for kaon pion pairs.

See Table 5.1 and the according plot. As a consequence of mixing, particles in the overlapping region could be taken as pion or kaon. Therefore the following algorithm is applied:

- If both particles are in their own bands, they are taken as unambiguous kaon pion pair.
- If one of them is in its own band but the other is in the ambiguous region, the latter is taken as suiting partner. For example if one particle above 2 GeV/c is in the Kaon band and the other one around 1 GeV/c in the overlapping region, the latter is taken as pion.
- If both particles are in the ambiguous region, the one closer to the kaon Bethe-Bloch line is taken as kaon and the other as pion.

The sigma values and the momentum borders are a first attempt. There is still room for optimization. After the identification of kaon pion pairs, those coming from D^0 's are tried to selected out of the many background sources of kaons and pions. Among the background are also kaons and pions coming from D^0 's but from another decay mode like $D^0 \rightarrow K^- \pi^+ \pi^0$ 13,9%. In order to suppress the background the following cut variables are used:

Kaon and Pion DCA Distance of closest approach in xy plane to the primary vertex of the kaon/pion track.

Kaon-Pion DCA Distance of closest approach in xy plane between kaon and pion tracks.

DCA Product Product of kaon and pion DCA's in xy plane.

Kaon and Pion p_t Transverse momentum of kaon/pion.

$\text{Cos}\theta_{pointing}$ Cosine of angle between the momentum vector of D^0 candidate, reconstructed out of the kaon pion pair, and the connection line (flight line) between primary and secondary vertex. Primary vertex is the position where the collision takes place. Secondary vertex is the position where the D^0 decays into its daughters.

$|\text{Cos}\theta^*$ | Decay Angle. Absolute of cosine of angle between D^0 direction and kaon or pion direction in the rest frame of D^0 .

$c\tau$ Decay length of D^0 .

\mathbf{p}_{rel} Difference of kaon and pion transverse momentum divided by D^0 candidate transverse momentum.

These cuts (except the latter two) are based on work, which is done in [Col06a]. The added two cut criteria are: The decay length and the relative momentum cut. Since the D^0 has a decay length of about 120 μm , the $c\tau$ cut helps to eliminate kaon and pion sources, coming from the primary vertex. Because of the primary vertex resolution, decay lengths can get negative values. A negative value means, that the decay vertex of the D^0 candidate is *behind* the reconstructed primary vertex. The relative momentum cut is based on the effect, that it characterizes the momentum correlation of the daughters in a 2-prong decay, compared to the background of kaon pion pairs having no momentum correlation, because of having different mother particles or having more prongs than two. It is computed in the following way: $(\mathbf{p}_t^K - \mathbf{p}_t^\pi) / p_t^{D^0}$. For tuning the cuts in order to maximize the significance of D^0 's, a global approach is necessary, since the cut variables are correlated and an independent single cut optimization can be incompatible with

$D^0 p_t$ Range (GeV/c)	0-1	1-3	3-5	>5
DCA Kaon (cm) <	0.05	0.1	0.05	0.05
DCA Pion (cm) <	0.05	0.1	0.05	0.05
DCA Kaon-Pion (cm) <	0.04	0.02	0.02	0.02
DCA Product (cm ²) <	-0.00025	-0.00025	-0.00015	-0.00015
p_t Kaon (GeV/c) >	0.55	0.8	0.8	0.8
p_t Pion (GeV/c) >	0.45	0.6	0.6	0.6
cos(Pointing Angle) <	0.7	0.8	0.8	0.9
cos(θ^*) <	0.8	0.8	0.8	0.8
Decay Length >	0	0	0	0
p_{rel} <	0.5	0.5	0.7	0.8

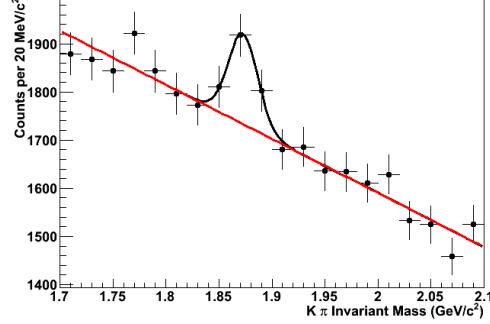
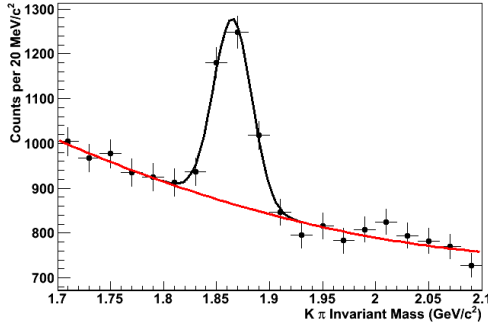
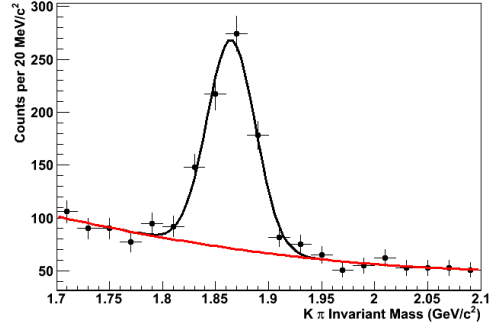
Table 5.2: Used cut values in order to obtain D^0 invariant mass distributions shown in Figure 5.1.

other cuts. For this purpose parallel coordinates [Cou08] were used, to apply a multidimensional and thus fully consistent tuning. The application and an excerpt of the tuning process is shown in Appendix A. The outcome of the tuning in order to maximize the statistical significance of D^0 's is listed in Table 5.2 for the available pass 2 data.

With this set of cut values the following invariant mass distributions are obtained: see Figure 5.1. The related signal and background informations and according statistical errors for the mentioned available pass 2 statistics are listed in Table 5.3. For the calculation 3 sigmas around the mean are considered for signal and background.

$p_t^{D^0}$ (GeV/c)	S	B	S/B	Significance
2-3	325±18	7238±85	0.040±0.002	3.74±0.21
3-5	930±30	4675±68	0.200±0.007	12.42±0.44
>5	560±24	488±22	1.150±0.244	17.30±3.67

Table 5.3: D^0 Reconstruction Performance with pass 2 data.

(a) Bin 3: $2 \rightarrow 3$ GeV/c. Mean = 1.873, $\sigma = 0.014$ (b) Bin 4: $3 \rightarrow 5$ GeV/c. Mean = 1.865, $\sigma = 0.017$ (c) Bin 5: $5 \rightarrow 7$ GeV/c. Mean = 1.865, $\sigma = 0.023$ Figure 5.1: D^0 Invariant mass distributions in 3 p_t bins with data from pass 2.

It is currently not possible to filter D^0 's out of the background in the lowest D^0 transverse momentum bin (0-1(GeV/c)). In the higher bins the D^0 peak is clearly visible. 1815 D^0 mesons in total could be reconstructed. This number can be improved with the same statistics by further tuning of the cuts and the kaon pion selection strategy in the TPC. As known, a selection of 1σ in the gaussian distribution around the dE/dx line, means leaving out more than 30% of the particles. A more inclusive cut can increase the D^0 statistics, for the price having a bigger pion contamination, which can lead to smaller signal to background ratios.

5.1.1 Conclusions from the D^0 Reconstruction

The D^0 raw yields, i.e. all reconstructed D^0 's in the full statistics, above 2 GeV/c and in p_t bins are shown in Figure 5.2. As the expression raw yield indicates, there are no reconstruction efficiencies considered here. In the Physics Working Group - Heavy Flavor and Quarkonia, within which this thesis also is, studies of the mentioned corrections, delivering distributions with absolute normalization

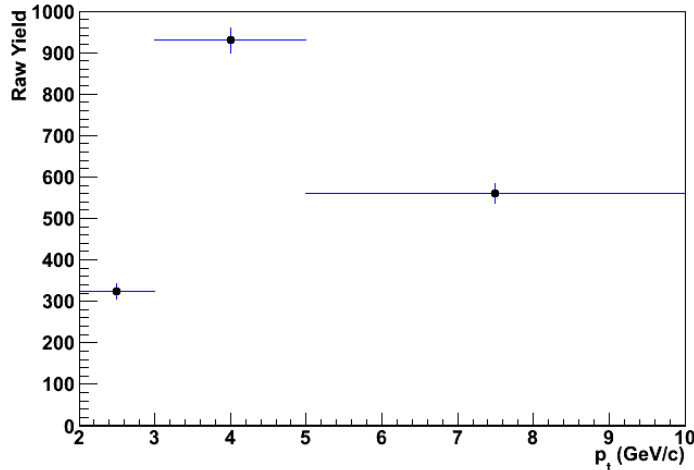


Figure 5.2: D^0 raw yields in 3 p_t bins.

are done (see Figure 5.3).

Heavy quarks are produced in hard processes, making perturbative QCD (pQCD) applicable. Therefore charm and bottom production can be calculated by employing pQCD, as it is the case in FONLL (Fixed-Order plus Next-to-Leading-Log) [CFM⁺04] and GM-VFNS (General-Mass Variable Flavor-Number Scheme) [KKSS05] calculations. The predictions of these calculations are compared to data in Figure 5.3. The mentioned theoretical predictions are within the errors in good agreement with data. These results have particular importance since these measurements provide a proof of success of pQCD in a new energy domain and contributes also to constrain the parameters of pQCD. In Figure 5.4 for instance, the total charm cross section per nucleon-nucleon collision for different experiments as a function of collision energy can be seen. At low and LHC energies the MNR (pQCD) calculation agrees with the data points within theoretical uncertainties and experimental errors, whereas at RHIC energies the agreement is only valid for the PHENIX but not for the STAR data point.

Taking the ratio of neutral D mesons and charged ones (reconstructed by the same physics working group mentioned), it is possible to make comparisons with the statistical model [ABBM⁺09]. The plot in Figure 5.5 shows the D^0/D^+ ratio as a function of p_t restricted to the rapidity interval $|y| < 0.5$. The red data point is the p_t integrated ratio. The same data point, again in red (full square), is visible in Figure 5.6, which shows additionally other data points for different energies, obtained by other experiments and the calculation according to the statistical model for elementary hadronic collisions. In order to understand the properties of the statistical model in nucleus-nucleus collisions, it is important to study the appli-

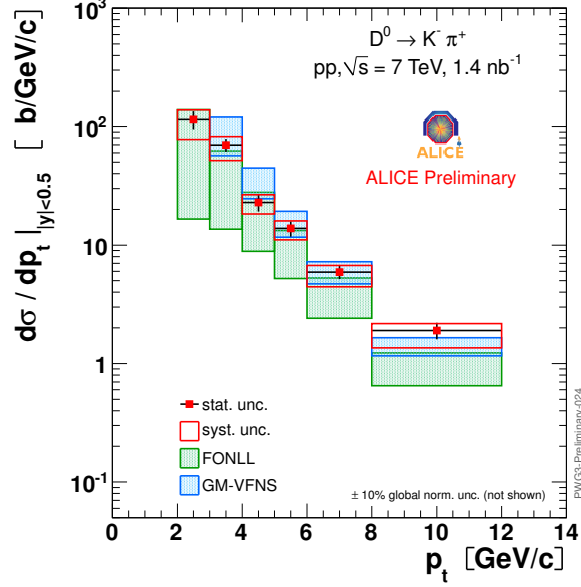


Figure 5.3: D^0 production cross section as function of p_t with statistical and systematic errors and comparison with FONLL and GM-VFNS calculations. The distributions are restricted to the rapidity interval $|y| < 0.5$. [Phyb]

cation of the statistical model to elementary hadron collisions, like pp collisions. As it can be seen in Figure 5.6, the ALICE data point is within the error in very good agreement with the prediction of the statistical model. The agreement in elementary collisions, where is no thermalization, shows, that it is not possible to distinguish any difference between pp and nucleus-nucleus collisions in the open charm sector [ABBM⁺09].

5.2 Electron Selection

Electrons are identified by using TPC and TOF. In the TPC a parametrized momentum dependent energy loss function rejecting hadrons is put as condition and in the TOF 3 σ 's around the expected time are required. The hadron contamination (or electron purity which is: Electron purity = 1 - Hadron contamination) reached by this strategy is on the percent level as seen in Figure 5.7. As explained in Chapter 2, the TRD can contribute significantly to the electron identification in the momentum region higher than 1 GeV/c. This will allow to extend the e - D^0 correlation analysis in the future to higher transverse momentum.

Since the electron coming from hadron decays occurs in semileptonic de-

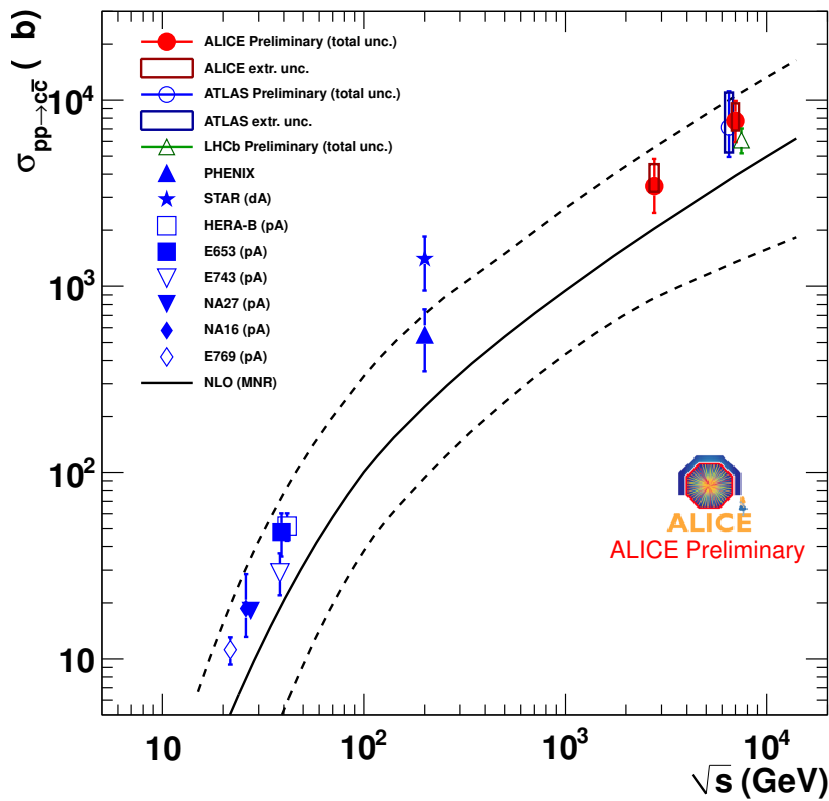


Figure 5.4: Measurements of experiments and MNR (pQCD) calculation for the total charm cross section per nucleon-nucleon collision as a function of center-of-mass system energy. The dashed lines represent the uncertainties of the MNR calculation. Since the ATLAS data point overlaps largely with the ALICE data point, it is slightly offset for clearness purposes. [Cole]

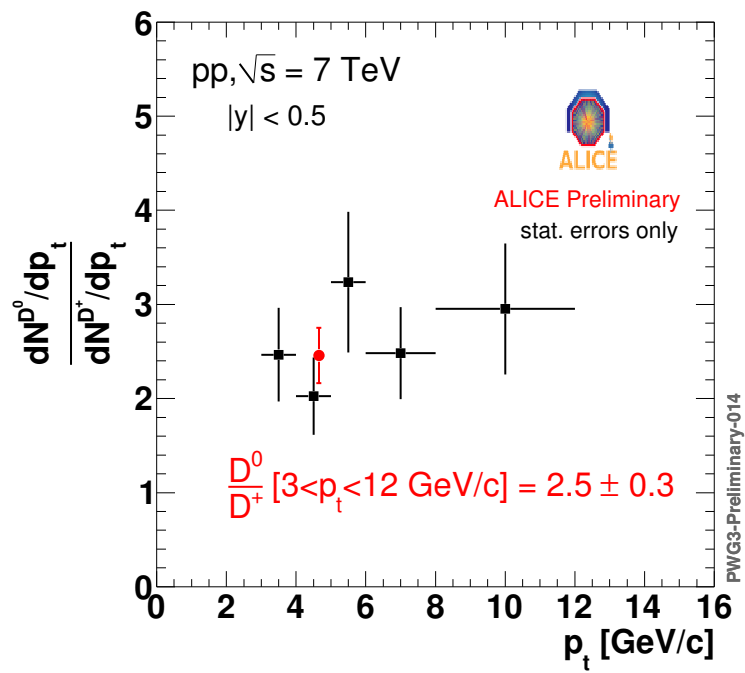


Figure 5.5: D^0/D^+ ratio as a function of p_t . Only D^0 and D^+ mesons in the range $3 < p_t < 12$ GeV/c are considered. The red data point represents the average of the mentioned transverse momentum range. [Phyb]

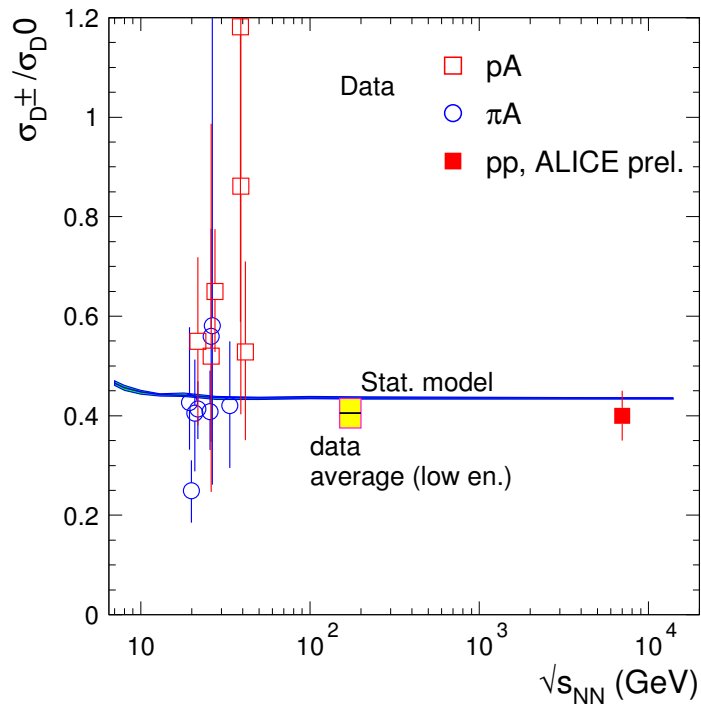


Figure 5.6: Charged to neutral D meson cross section ratios as function of center-of-mass energy in elementary hadron collisions with comparison to statistical model calculation. Red full square is the ALICE preliminary data point, which is not included in the data average shown as yellow box with corresponding error bar. The statistical model calculations are represented by the thin blue band and the other data points as empty squares or circles with color code according to the collision system. [ABBM⁺09], [DRa]

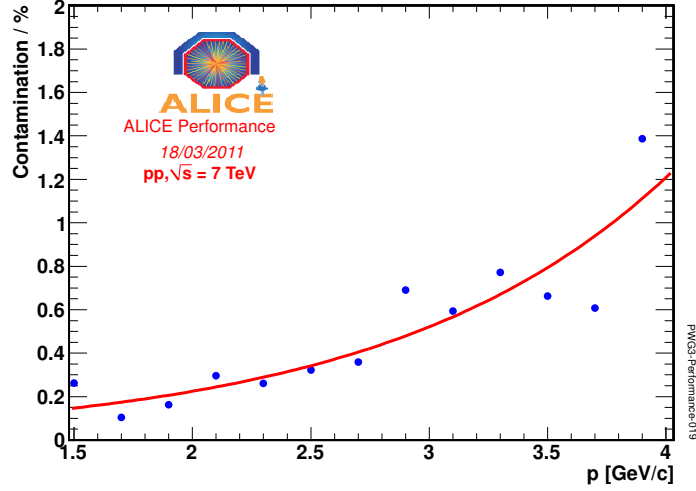


Figure 5.7: Hadron contamination (in percent) of electrons as a function of momentum, using the particle identification of the TOF and TPC detectors [Phyb].

cays, where it is always accompanied by a neutrino, the reconstruction of the mother particle is not possible. Therefore a definite assignment of an electron to D^0 or other charm containing hadron is unfeasible. An example decay mode is: $D^0 \rightarrow K^- e^+ \nu_e$ with a branching ratio of 3,58%. A possible method to enhance the heavy-flavor electron content, could be the requirement of an accompanying kaon. Beside kinematical constraints a strict condition on the invariant mass can be applied like: $m_{invariant}(D^0) > E_K + E_e$. To concentrate on a certain decay mode decreases the statistics significantly. In Figure 5.8 the evolution of entries vs. cuts, which lead to entries in the correlation distribution are displayed. As seen there, to be too selective with the requirement of a kaon and connected constraints, simply leads to an empty correlation plot, with the current statistics. Relaxing the conditions enables to obtain correlation entries but causes on the other hand a contamination with electrons, not originating from heavy flavor. Since the correlation is based on the condition that the electrons come from heavy flavor, the contamination has to be minimized (nevertheless, non-heavy-flavor electrons are subtracted on statistical basis later from the correlation distribution).

There are many electrons coming from non-heavy-flavor sources. These are mainly Dalitz decays or dielectron decays of $\pi^0, \eta, \omega, \eta', \phi, \rho, J/\psi, Y$ mesons, electrons from photon conversion in material and from direct and virtual direct photons. A cocktail, made out of the mentioned non-heavy-flavor electron sources is shown in Figure 5.9. The π^0 spectrum is taken from the reconstruction of photon conversions and based on that, the spectra of heavier mesons is obtained by

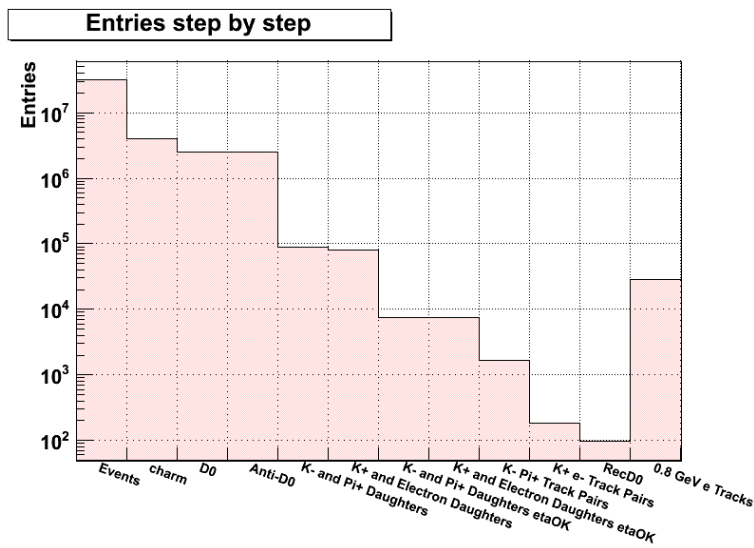


Figure 5.8: Evolution of entries vs. cuts. The steps are: Number of events, charm events, D^0 mesons, \bar{D}^0 mesons, decays in kaon and pion, decays in kaon and electron, kaons and pions in the ALICE coverage, kaons and electrons in the ALICE coverage, tracked kaons and pions, tracked kaons and electrons, reconstructed D^0 and \bar{D}^0 mesons, electron tracks with momentum higher than 0.8 GeV/c. The steps are not independent, they are computed, containing always the previous step, except the last column.

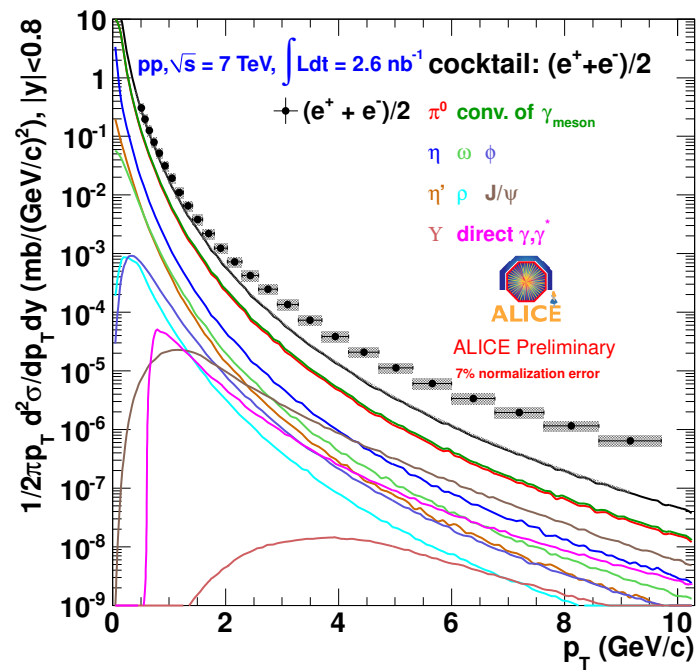


Figure 5.9: Inclusive electron spectrum and cocktail, containing non-heavy-flavor electron sources. The electron spectrum shows as expected, predominantly due to heavy-flavor electrons an excess over the cocktail especially at higher transverse momentum. [Colc]

m_T scaling [Mas11]. A significant contribution to the cocktail comes from photon conversions. Their amount is limited by requiring a hit in the first SPD layer, to reject conversions happening at larger radii. This leaves in the contributions from the beam pipe and partially from the first pixel layer itself. In the same Figure the inclusive electron spectrum measured in ALICE at midrapidity is shown. The excess of the inclusive spectrum compared to the cocktail is predominantly due to heavy-flavor electrons.

As mentioned above, the major sources of background electrons are gamma conversions and Dalitz decays. For the suppression of gamma conversion electrons and Dalitz decay electrons, an invariant mass cut of $0.150 \text{ GeV}/c^2$ is applied on dileptons. Additionally a decay length for electron positron pairs is calculated and pairs having a decay length greater than 3 cm, are tagged as background. In order to catch single-track conversions first very loose conditions are required for electron tracks (only TPC particle identification). After the identification of background pairs, all primarily mentioned single track cuts are applied plus the requirement of a hit in the first SPD detector layer. By this preliminary strategy a heavy-flavor to inclusive electron ratio of 26% is achieved. This ratio is at the level of experiments doing also e - D^0 correlations, like for example presented in [MtSC08].

It is possible to increase the heavy-flavor electron content by requiring a minimum transverse momentum condition. The effect from such a cut alone can be read from Figure 5.10. According to the ratio, shown in the Figure, at $2 \text{ GeV}/c$ electron momentum a heavy-flavor electron content of roughly 43% is present. In order to catch a first glimpse of correlations, the threshold is set to $0.5 \text{ GeV}/c$.

5.3 Correlation Analysis

As mentioned in the previous section, the selected electrons have a certain contribution from non-heavy-flavor sources. However the non-heavy-flavor content of electrons entering the correlations will be reduced because of the following: Since a correlation entry requires also the presence of a D^0 , the according event must be an event with charm production. Because of flavor conservation, charm quarks are produced as pairs and if a D^0 is identified, it is possible to calculate the probability, that the other charm quark hadronizes and decays into an electron. The $PIF(c \rightarrow e^+, \diamond, [P])$, explained in section 3.2, without momentum restriction, is roughly 0.005, which means roughly 0.5% of charm events will have an identified heavy-flavor positron (Background suppression is included). Moreover by this number it is possible to estimate, the expected number of entries in the correlation distributions. For the correlations only D^0 mesons with transverse momentum higher than $3 \text{ GeV}/c$ are taken into account, since in the lower p_t bin,

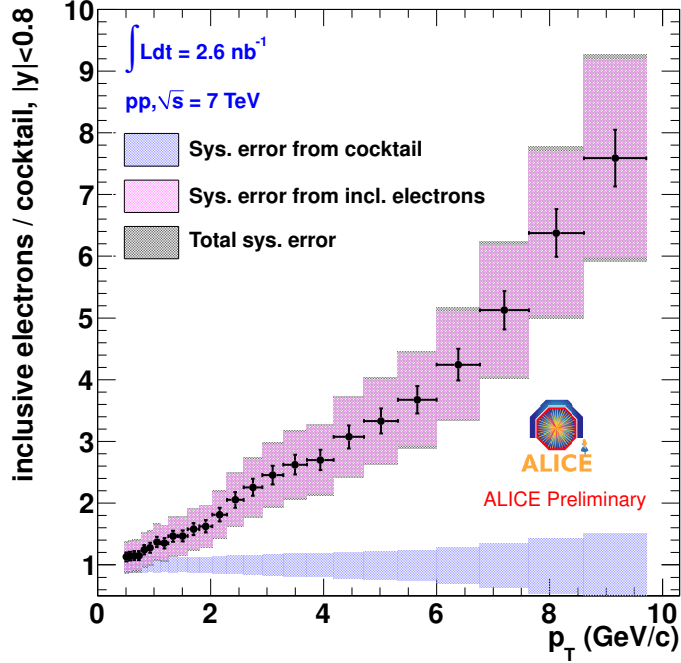


Figure 5.10: Ratio obtained from inclusive electron spectrum and cocktail as a function of p_t [Cold].

the signal to background ratio is rather low. In sum there are 1490 D^0 mesons in the mentioned higher p_t bins. This number multiplied by the PIF is the expected number of entries, namely roughly 7. This estimation shows, that unfortunately with the current statistics, a clear statement about charm to beauty ratios is not possible. Nevertheless a first computation is done, keeping in mind the mentioned uncertainty. In Figures 5.11-5.14 first correlation entries with pass 2 statistics of about a quarter billion events are presented. The correlation distributions are obtained by correlating selected electrons in azimuthal angle with D^0 mesons inside the peak region (within 3 sigma around the mean value) or the sidebands (vicinity on two sides next to the peak region, having a normalized area to the area below the polynomial fit (red in Figure 5.1) in the peak region) and combining them, described in the following:

The distribution in Figure 5.11, which is the correlation of selected electrons with D^0 candidates in the peak region, contains the following contributions:

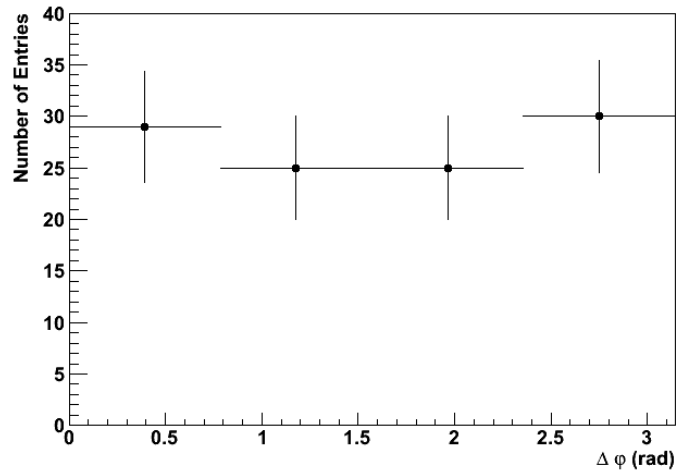


Figure 5.11: Electrons correlated with D^0 candidates in the peak region.

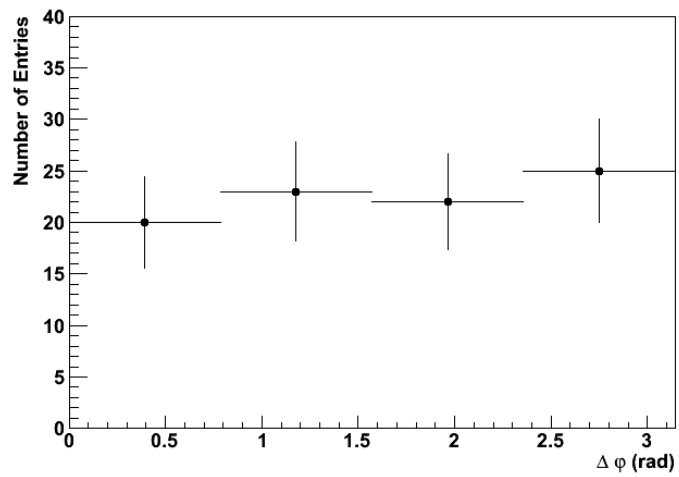
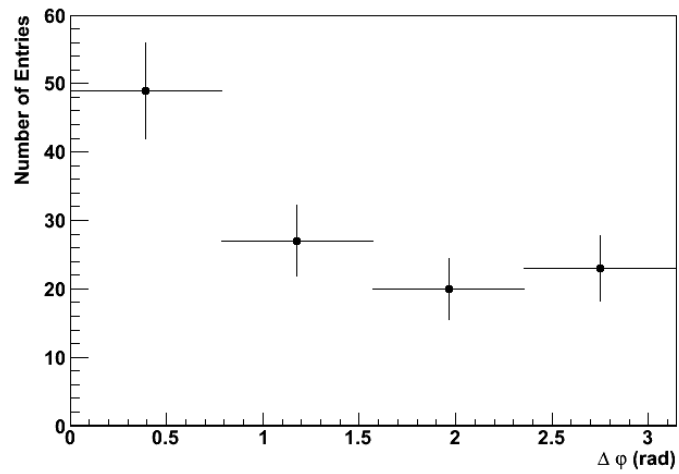
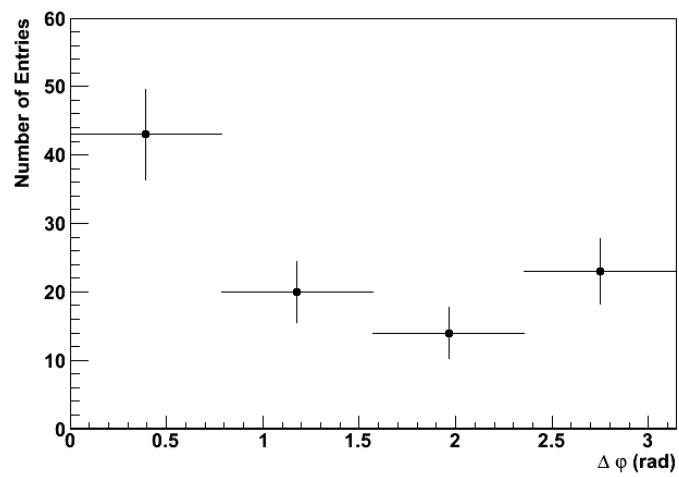


Figure 5.12: Electrons correlated with D^0 candidates in the sideband.

Figure 5.13: Electrons correlated with \bar{D}^0 candidates in the peak region.Figure 5.14: Electrons correlated with \bar{D}^0 candidates in the sideband.

HFE- D^0 Heavy-Flavor Electrons - D^0 's.

HFE-p D^0 Heavy-Flavor Electrons - pseudo D^0 's.

NHFE- D^0 Non-Heavy-Flavor Electrons - D^0 's.

NHFE-p D^0 Non-Heavy-Flavor Electrons - pseudo D^0 's.

Since hadrons, which are misidentified as electrons are, as shown in Figure 5.7, on the percent level, they are not explicitly mentioned here but counted currently as approximation among the NHFE component. The latter three contributions listed above, have to be subtracted from the overall distribution in order to obtain purely HFE- D^0 correlations.

As first step, the sideband correlation, obtained from the correlation of electrons with D^0 candidates in the sideband, in Figure 5.12 is subtracted from the correlation in Figure 5.11. By this the HFE-p D^0 and NHFE-p D^0 contributions are removed and only the NHFE- D^0 contribution remains to be subtracted. If the electrons could be selected such that they are purely of heavy-flavor origin, the next steps would be obsolete and the two type of correlations (e- D^0 and e- \bar{D}^0) could be evaluated independently, as described in the method in section 4.3. Another way of enabling an individual evaluation of Correlation Type I and II, is possible by performing the subtraction, using simulations. Since this would introduce additional angular dependencies, a data oriented strategy is preferred which is described in the following:

In order to get rid of the remaining NHFE- D^0 contribution, a further step has to be applied and the application of the mentioned method in section 4.3 has to be adapted. First the same subtraction procedure like above is applied for the correlation type II (e- \bar{D}^0 pairs). After this, here the NHFE- \bar{D}^0 contribution remains to be subtracted. The obtained values for the two correlation types are shown in Table 5.4 (with only statistical errors).

Angular Bin	$0 - \frac{\pi}{4}$	$\frac{\pi}{4} - \frac{\pi}{2}$	$\frac{\pi}{2} - \frac{3\pi}{4}$	$\frac{3\pi}{4} - \pi$
Selected electron- D^0	9 ± 7.0	2 ± 6.9	3 ± 6.9	5 ± 7.4
Selected electron- \bar{D}^0	6 ± 9.6	7 ± 6.9	6 ± 5.8	0 ± 6.8

Table 5.4

After obtaining the selected electron- D^0 and selected electron- \bar{D}^0 correlations, the latter is subtracted from the first (The normalization of the distributions

before the subtraction drops by the assumption of equal D^0 and \bar{D}^0 reconstruction efficiency). Since the NHFE component should be independent of being correlated with D^0 or \bar{D}^0 , it is assumed that the NHFE- D^0 and NHFE- \bar{D}^0 correlations have equal angular properties. Under this assumption, the mentioned two contributions cancel in the subtraction and a final angular distribution, which corresponds to the difference of the HFE- D^0 and HFE- \bar{D}^0 distributions, remains.

The evaluation procedure described in section 4.3 has to be adapted accordingly. Instead of evaluating type I and II individually, all contributions from Quarter c are subtracted from Quarter a and the ones from Quarter d are subtracted from Quarter b, which means the subtraction of equation 4.3 from 4.1 and the subtraction of equation 4.4 from 4.2. The obtained new set of equations are solved then with the difference values written in Table 5.4. With the current values listed in the mentioned table the computed charm to beauty ratio is unphysical. The errors of the obtained values, again visible in Table 5.4, are in the order of the obtained values, which means there is simply no statistical significance yet. Assuming a flat angular correlation distribution and linear scaling of the signal to background ratio of reconstructed D^0 mesons, for the purpose of error estimation, with one billion events, the relative error would shrink to roughly 27 %. This would allow first statements with certain statistical significance. Improvements like the detector calibration, particle identification performance, improved selection cuts, inclusion of lower D^0 p_t bins and the possibility of triggering are not considered in the projection to a billion events, which will enhance the correlation statistics.

Systematic dependencies cancel partially out, since a ratio of reconstructed e- D^0 pairs with other reconstructed e- D^0 pairs in a different angular region is taken. However the cuts used for the D^0 reconstruction have a different impact on D^0 mesons originating from charm or beauty. Since B mesons have a roughly 4 times larger decay length, the kinematical observables of D^0 mesons do change, depending on original flavor. For the other cut variables similar considerations are valid. These dependencies were not possible to study, with the present low statistics.

Chapter 6

Conclusion and Outlook

First neutral D meson measurements have been performed in pp collisions at 7 TeV center-of-mass energy. Using the powerful capabilities of ALICE a clear identification of D mesons down to low p_t is possible. Such measurements provide strong tests of pQCD. Preliminary comparisons of pQCD with obtained spectra show agreement.

For performing e- D^0 correlations, in addition to the reconstruction of D^0 mesons, electrons coming from heavy-flavor sources, have to be selected. For this purpose a successful strategy is worked out.

The focus in this work is on the angular correlations of electrons with neutral D mesons. For this purpose analysis methods have been worked out and a new method, called factorization method is proposed. Also a novel background subtraction method is applied. First computations for the charm to beauty cross section ratio show, that a safe statement (described in section 5.3) awaits the high statistics analysis which will be performed with the events, recorded and reconstructed within most probably 2011, which is the next step.

Beside the charm to beauty cross section ratio, the results will also provide a cross check with another technique of charm to beauty cross section ratio measurement, which is based on the displacement with respect to the vertex of electrons depending on their original charm or beauty flavor. A further perspective is the investigation of angular distributions of QCD processes.

Appendix A

Parallel coordinates

Parallel coordinates are a comfortable way to study multiple variable data sets [Cou08]. Instead of perpendicular axes, known from Cartesian coordinates, parallel ones are used. This allows a representation in more than three dimensions. A point in n-dimensional space is shown by a polyline with vertices on the axes. The vertex position on the axis represents the value of the point in this coordinate. As an simple example, in Figure A.1 the six dimensional point $(-5,3,4,2,0,1)$ is drawn. Transferring this tool to our cut tuning purpose means, representing each cut variable listed in section 5.1 above as an axis in parallel coordinates. Each polyline, connected to certain values on the axes, represents a data point. In Figure A.2 only an excerpt of the tuning process is shown, because of the so-called *cluttering* effect (The histogram gets quickly opaque, due to display problems of many lines). The functionality is provided by the class TParallelCoord of root ([Roo]). It is possible to zoom in and out independently at each axis. The range selection can be done via sliders, depicted as triangles. By moving the sliders, ranges can be included or excluded and the polylines appear or disappear accordingly. By this functionality the signal to background ratio can be improved and

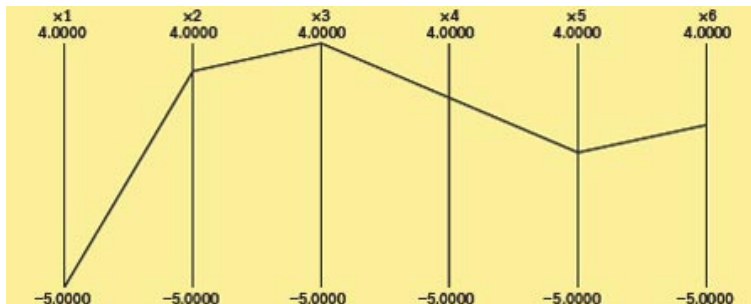


Figure A.1: Example six dimensional point $(-5,3,4,2,0,1)$ in parallel coordinates.

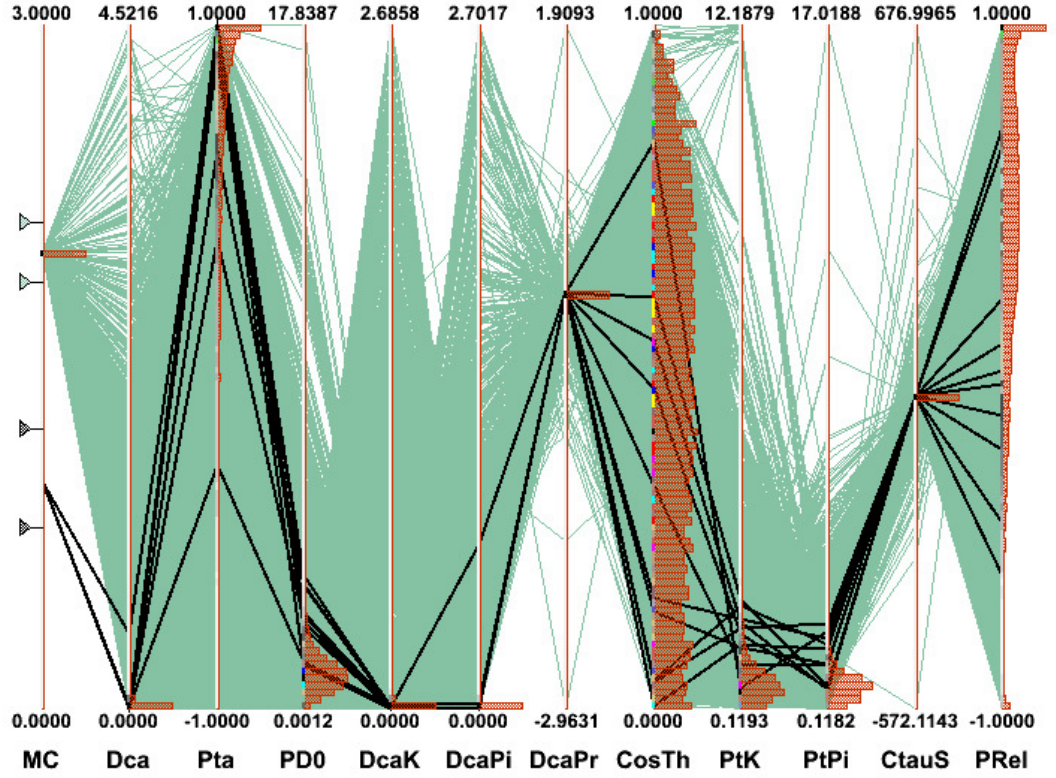


Figure A.2: Parallel coordinates used in order to tune globally the selection D^0 cuts. The axis are from left to right: Monte Carlo truth (1:Signal and 2:Background), Kaon-Pion DCA, $\text{Cos}\theta_{\text{pointing}}$, $p_t^{D^0}$, Kaon DCA, Pion DCA, DCA Product, $\text{Cos}\theta^*$, Kaon p_t , Pion p_t , $c\tau/\sigma$, p_{rel} . Color code is: Green: Background, Black: Signal. At top and bottom of the axes, the ranges are displayed.

moreover correlations between cut variables can be recognized. A histogram on each axis, supports the displaying of all entries.

After obtaining a global setting, nevertheless for fine-tuning purposes, cuts are tuned independently. Despite the impressive capabilities of the parallel coordinates, it has the limitation, not being able to handle too many data points. Half a million entries are a kind of effective limit. However the limitation can be partially overcome, by using enhanced data samples and adjusted binning of the axes.

Appendix B

Single contribution type for Factorization Method

The correlation function used in the factorization method (see section 4.3) arises from the angular relation of e - D^0 pairs, which are a result of a chain of processes. Each combination of processes makes an individual contribution, which represents the probability of $c\bar{c}$ or $b\bar{b}$ occurrence in the according angular region. In Figure 4.7 and 4.8 possible main contribution types are listed. In order to explain the come about of a single contribution type, an example process chain (tag number 3 in Quarter b in Figure 4.7) is illustrated in Figure B.1. The process starts obviously with the production of the $b - \bar{b}$ pair, nevertheless for explanation purposes the process chain is described in the following, beginning from right with the electrons. The single quantities are:

- Branching ratio of \bar{B}^0 decaying into electrons.
- Reduction of \bar{B}^0 mesons because of B^0/\bar{B}^0 oscillation.
- Branching ratio of b quarks fragmenting into \bar{B}^0 .

The upper processes are a certain sequence of processes. However there are many possibilities that a b quark fragments into an electron. All these possibilities are combined as $PIF(b \rightarrow e^-, \diamond, [P])$, explained in section 3.2, in one quantity. This is in contrast to the D^0 side, where only a single process chain is considered for one contribution type. By using the PIF also reconstruction efficiencies and moreover applied background suppression can be incorporated, which are represented as diamond in the PIF nomenclature.

- $b\bar{b}$ production cross section with away side (between $\frac{\pi}{2}$ and π) orientation. In this example the underlying QCD process is pair creation. In fact the sum

of all processes with away side orientation can be taken for this contribution. The production cross section is considered unknown and the angular information can be obtained from simulations. The values obtained from PYTHIA and MNR are listed further below.

- Branching ratio of \bar{b} quarks fragmenting into B^0 .
- Reduction of B^0 mesons because of B^0/\bar{B}^0 oscillation.
- Branching ratio of B^0 decaying into D^0 mesons (This decay mode is Cabibbo suppressed (CS)).
- Reduction of D^0 mesons because of D^0/\bar{D}^0 oscillation. Has very low impact but is mentioned here for completeness purposes.
- Reduction because of CP violation in decay. Has minor impact.

Calculation Ingredients

Values which are included for the calculation of various single contributions are listed here:

- $PIF(c \rightarrow e^-, \diamond) \approx 0.0000362$
- $PIF(c \rightarrow e^+, \diamond) \approx 0.00491$
- $PIF(b \rightarrow e^-, \diamond) \approx 0.00773$
- $PIF(b \rightarrow e^+, \diamond) \approx 0.00157$

The diamond in the PIF represents ALICE acceptance, reconstruction efficiencies and background suppression, applied as described in section 5.2.

- The reconstruction (and identification) efficiency of an electron which occurs, because it is in company of a D^0 coming from the same decay chain ($B^- \rightarrow e^- \nu_e D^{*0} (\rightarrow D^0 X)$) is ≈ 0.18 .
- All particle branching ratios used in calculations here, are from [Aea08].

- The production probabilities of heavy-quark pairs according to their relative angle in φ (NS:Near-side, AS: Away-side) are listed in the table below. The values do not contain momentum selections. Since in the e- D^0 correlations both electrons and D^0 's are selected according to their transverse momentum, the simulations have to be adapted. In this analysis all D^0 transverse momentum bins are included and also for electrons a low p_t cut is applied. Therefore nevertheless the values below are used as a first approach.

Flavor	charm		beauty	
	NS ($0 - \frac{\pi}{2}$)	AS ($\frac{\pi}{2} - \pi$)	NS ($0 - \frac{\pi}{2}$)	AS ($\frac{\pi}{2} - \pi$)
PYTHIA \approx	0.39	0.61	0.35	0.65
MNR \approx	0.69	0.31	0.23	0.77

Table B.1

Bibliography

- [A⁺10] J. Alme et al. The ALICE TPC, a large 3-dimensional tracking device with fast readout for ultra-high multiplicity events. *Nucl. Instrum. Meth.*, A622:316–367, 2010.
- [Aam10] K. et al. Aamodt. Charged-particle multiplicity density at midrapidity in central pb-pb collisions at $\sqrt{s_{NN}} = 2.76$ tev. *Phys. Rev. Lett.*, 105(25):252301, Dec 2010.
- [ABBM⁺09] A. Andronic, F. Beutler, P. Braun-Munzinger, K. Redlich, and J. Stachel. Statistical hadronization of heavy flavor quarks in elementary collisions: Successes and failures. *Physics Letters B*, 678(4):350 – 354, 2009.
- [ABMS10] A. Andronic, P. Braun-Munzinger, and J. Stachel. The horn, the hadron mass spectrum and the qcd phase diagram - the statistical model of hadron production in central nucleus-nucleus collisions. *Nuclear Physics A*, 834(1-4):237c – 240c, 2010. The 10th International Conference on Nucleus-Nucleus Collisions (NN2009).
- [ACD⁺06] Néstor Armesto, Matteo Cacciari, Andrea Dainese, Carlos A. Salgado, and Urs Achim Wiedemann. How sensitive are high-pt electron spectra at RHIC to heavy quark energy loss? *Physics Letters B*, 637(6):362 – 366, 2006.
- [Aea06] S. S. Adler et al. Single Electrons from Heavy-Flavor Decays in $p + p$ Collisions at $\sqrt{s} = 200$ GeV. *Phys. Rev. Lett.*, 96(3):032001, Jan 2006.
- [Aea08] C. Amsler et al. Review of particle physics. *PHYSICS LETTERS B*, 667:1-5, s. 1-, 2008.
- [Aea10] M. M. Aggarwal et al. Measurement of the Bottom Quark Contribution to Nonphotonic Electron Production in $p + p$ Collisions at $\sqrt{s} = 200$ GeV. *Phys. Rev. Lett.*, 105(20):202301, Nov 2010.

- [BDM⁺97] R. Baier, Yu. L. Dokshitzer, A. H. Mueller, S. Peign, and D. Schiff. Radiative energy loss of high energy quarks and gluons in a finite-volume quark-gluon plasma. *Nuclear Physics B*, 483(1-2):291 – 320, 1997.
- [Bea81] M. Basile et al. Measurement of associated production of $D^0 \bar{D}$ in pp Interactions at $\sqrt{s} = 62$ GeV. *Il Nuovo Cimento A (1971-1996)*, 65:457–469, 1981. 10.1007/BF02902049.
- [CFM⁺04] Matteo Cacciari, Stefano Frixione, Michelangelo L. Mangano, Paolo Nason, and Giovanni Ridolfi. QCD analysis of first b cross section data at 1.96 TeV. *Journal of High Energy Physics*, 2004(07):033, 2004.
- [CNV05] Matteo Cacciari, Paolo Nason, and Ramona Vogt. QCD Predictions for Charm and Bottom Quark Production at RHIC. *Phys. Rev. Lett.*, 95(12):122001, Sep 2005.
- [Cola] ALICE Collaboration. ALICE Offline Pages, The Analysis Framework, Physics Event Selection. <http://aliweb.cern.ch/Offline/Activities/Analysis/AnalysisFramework/index.html>.
- [Colb] ALICE Collaboration. dE/dx spectrum versus momentum in the ALICE TPC for 7 TeV pp collisions. <http://aliceinfo.cern.ch/>. Figure Repository.
- [Colc] ALICE Collaboration. Inclusive electron spectrum and cocktail. <http://aliceinfo.cern.ch/>. Figure Repository.
- [Cold] ALICE Collaboration. Ratio of inclusive spectrum over cocktail. <http://aliceinfo.cern.ch/>. Figure Repository.
- [Cole] ALICE Collaboration. Total charm production cross section vs c.m.s. energy, compared also to ATLAS and LHCb. <http://aliceinfo.cern.ch/>. Figure Repository.
- [Col04] ALICE Collaboration. ALICE: Physics Performance Report, Volume I. *Journal of Physics G: Nuclear and Particle Physics*, 30(11):1517, 2004.
- [Col06a] ALICE Collaboration. ALICE: Physics Performance Report, Volume II. *Journal of Physics G: Nuclear and Particle Physics*, 32(10):1295, 2006.

-
- [Col06b] ALICE Collaboration. ALICE: Physics Performance Report, Volume II. *Journal of Physics G: Nuclear and Particle Physics*, 32(10):1295, 2006. Illustration by Hongyan Yang.
- [Col08a] J Coleman. $D^0 \bar{D}^0$ mixing at BaBar. *Journal of Physics: Conference Series*, 110(5):052009, 2008.
- [Col08b] The ALICE Collaboration. The ALICE experiment at the CERN LHC. *Journal of Instrumentation*, 3, 2008.
- [Col11] The ALICE Collaboration. Suppression of charged particle production at large transverse momentum in central Pb-Pb collisions at $\sqrt{s_{NN}} = 2.76$ tev. *Physics Letters B*, 696(1-2):30 – 39, 2011.
- [Cou08] O. Couet. Multiple variables data sets visualization in ROOT. *Journal of Physics: Conference Series*, 119(4):042007, 2008.
- [DK01] Yu. L. Dokshitzer and D. E. Kharzeev. Heavy-quark colorimetry of QCD matter. *Physics Letters B*, 519(3-4):199 – 206, 2001.
- [DKT91] Yu L Dokshitzer, V A Khoze, and S I Troyan. On specific QCD properties of heavy quark fragmentation ('dead cone'). *Journal of Physics G: Nuclear and Particle Physics*, 17(10):1602, 1991.
- [Dol92] Boris Dolgoshein. Transition radiation detectors. *Nuclear Instruments and Methods in Physics Research Section A*, pages 434–469, 19 July 1992.
- [DRa] Private communication Anton Andronic, GSI Helmholtzzentrum für Schwerionenforschung.
- [FK04] Zoltan Fodor and Sandor D. Katz. Critical point of QCD at finite T and μ , lattice results for physical quark masses. *Journal of High Energy Physics*, 2004(04):050, 2004.
- [FM04] R.J. Fries and B. Müller. Heavy ions at LHC: Theoretical issues. *The European Physical Journal C - Particles and Fields*, 34:s279–s285, 2004. 10.1140/epjcd/s2004-04-026-6.
- [GW73] David J. Gross and Frank Wilczek. Ultraviolet Behavior of Non-Abelian Gauge Theories. *Phys. Rev. Lett.*, 30(26):1343–1346, Jun 1973.

- [KKSS05] B. A. Kniehl, G. Kramer, I. Schienbein, and H. Spiesberger. Collinear subtractions in hadroproduction of heavy quarks. *The European Physical Journal C - Particles and Fields*, 41:199–212, 2005. 10.1140/epjc/s2005-02200-7.
- [Lex00] *Lexikon der Physik*, volume 4. Spektrum Akademischer Verlag GmbH, Heidelberg, 2000. ISBN 3-8274-1462-8.
- [Mas11] S. Masciocchi. Inclusive electron spectrum from heavy-flavour decays in proton-proton collisions at $\sqrt{s} = 7 \text{ TeV}$ measured with ALICE at LHC. *Nuclear Physics A*, 855(1):432 – 435, 2011. Proceedings of the 4th International Conference on Hard and Electromagnetic Probes of High-Energy Nuclear Collisions - HP2010.
- [MftSC08] André Mischke and for the STAR Collaboration. Heavy-flavor correlation measurements via electron azimuthal correlations with open charm mesons. *Journal of Physics G: Nuclear and Particle Physics*, 35(4):044022, 2008.
- [Mis09] André Mischke. A new correlation method to identify and separate charm and bottom production processes at RHIC. *Physics Letters B*, 671(3):361 – 365, 2009.
- [MNR] Private communication Anton Andronic, GSI Helmholtzzentrum für Schwerionenforschung.
- [MNR92] Michelangelo L. Mangano, Paolo Nason, and Giovanni Ridolfi. Heavy-quark correlations in hadron collisions at next-to-leading order. *Nuclear Physics B*, 373(2):295 – 345, 1992.
- [MtSC08] André Mischke and the STAR Collaboration. Heavy-flavor particle correlations in STAR via electron azimuthal correlations with D^0 mesons. *Journal of Physics G: Nuclear and Particle Physics*, 35(10):104117, 2008.
- [NA4] Main findings of NA49. <http://na49info.web.cern.ch/na49info/Public/Press/findings.html>.
- [Nac86] Otto Nachtmann. *Phänomene und Konzepte der Elementarteilchenphysik*. Vieweg Verlag, 1986. ISBN 3-528-08926-1.
- [NDH⁺11] Harri Niemi, Gabriel S. Denicol, Pasi Huovinen, Etele Molnar, and Dirk H. Rischke. Influence of the shear viscosity of the quark-gluon plasma on elliptic flow in ultrarelativistic heavy-ion colli-

-
- sions. *arXiv:1101.2442v1 [nucl-th]*, January 2011. Value converted from $T_{Max} = 598$ MeV.
- [Otw11] Jacek Otwinowski. Charged particle production at large transverse momentum in PbPb collisions at $\sqrt{s} = 2.76$ TeV measured with ALICE at the LHC. XXII International Conference On Ultra-Relativistic Nucleus-Nucleus Collisions, May 2011.
- [Phya] Physics Working Group 1 of the ALICE Collaboration. <http://aliweb.cern.ch/Physics/PWG1/index.html>.
- [Phyb] Physics Working Group 3 of the ALICE Collaboration. <http://aliweb.cern.ch/Physics/PWG3/index.html>.
- [Pol73] H. David Politzer. Reliable perturbative results for strong interactions? *Phys. Rev. Lett.*, 30(26):1346–1349, Jun 1973.
- [Roo] Root. <http://root.cern.ch>.
- [SAC⁺] Torbjörn Sjöstrand, Stefan Ask, Richard Corke, Stephen Mrenna, and Peter Skands. Webpage of PYTHIA. <http://home.thep.lu.se/torbjorn/Pythia.html>.
- [SW03] Carlos A. Salgado and Urs Achim Wiedemann. Calculating quenching weights. *Phys. Rev. D*, 68(1):014008, Jul 2003.
- [Tea] NASA / WMAP Science Team. Cosmic microwave background radiation. <http://map.gsfc.nasa.gov/media/080997/index.html>; http://map.gsfc.nasa.gov/news/5yr_release.html.
- [Won94] Cheuk-Yin Wong. *Introduction to High-Energy Heavy-Ion Collisions*. World Scientific Publishing Co. Pte. Ltd, 1994.
- [YHM05] Kohsuke Yagi, Tetsuo Hatsuda, and Yasuo Miake. *Quark-Gluon Plasma*. Cambridge University Press, 2005. ISBN-13 978-0-521-56108-2.

Acknowledgment

I thank everybody who made this thesis possible and would like to emphasize the following people:

My personal thanks goes to my family, who mastered together with me my PhD marathon.

I would like to express my deepest gratitude to Prof. Peter Braun-Munzinger who is the key person opening me the door to such an exciting experiment and allowing me to know all the people listed below and more. He trusted and supported me at all times, which reminded me always the german expression Doktorvater in its true meaning.

It was a privilege for me that Dr. Anton Andronic took care of my work from the very first and gave me the possibility to benefit from his impressive scientific experiences. I will always remember his very kind way even in critical situations and I have to note, that I have learned from him not only about physics. I compress pages of thanks to this sentence for mentoring me so sincerely.

I'm most grateful to Dr. Silvia Masciocchi for guiding me skillfully through complicated paths of data analysis and my PhD in general. It is not that she only supervised me excellently. It is that I felt always, that she took care of me, which is a reflection of her remarkable personality.

I thank greatly Prof. Henner Büsching for all educational activities within the H-QM school, for being a friend and giving me the opportunity to find many friends. I include all H-QM participants for my many thanks for the nice moments but have to mention my dear friend Dr. Attilio Tarantola explicitly. I'm also very grateful to Prof. Bengt Friman, who participated in my H-QM PhD committee.

Very special thanks to my office mates Benjamin Dönigus and Dr. Juan Castillo. Beside the invaluable discussions, help and feedback I got, they provided the perfect mood in our office.

I owe great gratitude to another office mate Anar Manafov, who contributed to my thesis significantly, by solving computing problems, which seemed to be unsolvable to me. In the same line I thank Markus Fasel, who helped me also in many tricky computing issues.

I am indebted to Dr. Alexandru Bercuci to support me tremendously in the data analysis of the TRD test beam data.

Moreover many many thanks for helping in several issues, having nice discussions and inspiring new ideas to Dr. Ralf Averbeck, Prof. Carlo Ewerz, Dr. Anar Rustamov, Alexander Kalweit, Dr. Rosella Romita, Dr. Ionut Arsene, Dr. Georgios Tsiledakis, Dr. Raphaele Bailhache, Dr. Woo Jin Park, Dr. Marian Ivanov, Dr. Dariusz Miskowicz and Prof. Helmut Öschler.

I would like to thank to Dr. Christian Schmidt and Jörg Hehner for the great help and support managing the logistics of TRD chamber parts.

I have to thank our secretary Sandra Schecker, who is not only amazingly helpful, she is very skilled in solving most tricky organisational issues.

Last but not least I would like to thank for creating a beautiful working atmosphere to my friends and colleagues Mesut Arslanok, Cahit Ugur, Jochen Thäder, Dr. Ingrid Kraus, Dr. Ana Marin, Dr. Jacek Otwinowski, Dr. Sergej Yurevich, Dr. Helene Ricaud, Michael Knichel, Markus Köhler, Dr. Ilya Selyuzhenkov, Dr. Ulrich Frankenfeld, Prof. Hans Rudolf Schmidt and others.

Eidesstaatliche Erklärung

Hiermit erkläre ich eidesstaatlich, dass ich die vorliegende Dissertation selbstständig verfasst, keine anderen als die angegebenen Hilfsmittel verwendet und noch keinen Promotionsversuch unternommen habe.

Darmstadt, den

gez. Sedat Altınpınar

Curriculum Vitae

Sedat Altınpınar

PERSONAL INFORMATION

Born on 14.9.73 in Wülfrath/Germany

Turkish Nationality

EDUCATION & PROFESSIONAL EXPERIENCE

2006-2011 PhD at GSI Helmholtzzentrum für Schwerionenforschung, Darmstadt, Germany. Thesis Title: Electron- D^0 correlations with ALICE in pp collisions at LHC energy.

1997-2006 Employment as student trainee and later in R&D at Siemens VDO Automotive AG.

1996-2006 Diplom study in Physics, Technical University of Darmstadt, Darmstadt, Germany. Thesis Title: Investigations of the Performance of ALICE TRD Chambers.

1993-1996 Diplom study in Physics, RWTH Aachen University, Aachen, Germany

1993-1993 Physics study, Middle East Technical University, Ankara, Turkey